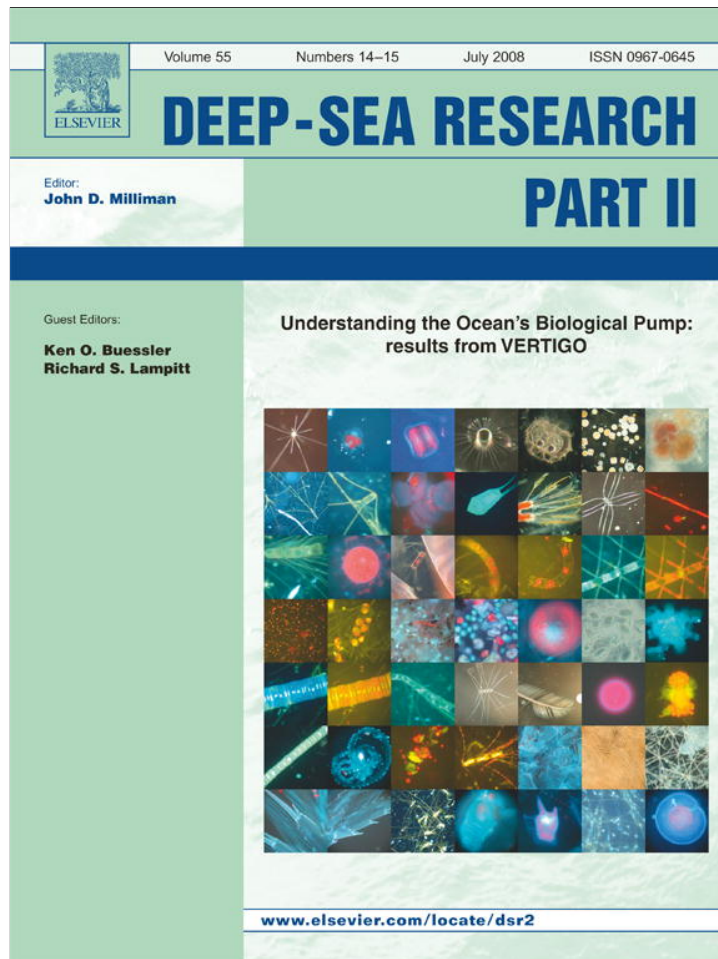


Provided for non-commercial research and education use.  
Not for reproduction, distribution or commercial use.



This article appeared in a journal published by Elsevier. The attached copy is furnished to the author for internal non-commercial research and education use, including for instruction at the authors institution and sharing with colleagues.

Other uses, including reproduction and distribution, or selling or licensing copies, or posting to personal, institutional or third party websites are prohibited.

In most cases authors are permitted to post their version of the article (e.g. in Word or Tex form) to their personal website or institutional repository. Authors requiring further information regarding Elsevier's archiving and manuscript policies are encouraged to visit:

<http://www.elsevier.com/copyright>



Contents lists available at ScienceDirect

## Deep-Sea Research II

journal homepage: [www.elsevier.com/locate/dsr2](http://www.elsevier.com/locate/dsr2)

# The flux of bio- and lithogenic material associated with sinking particles in the mesopelagic “twilight zone” of the northwest and North Central Pacific Ocean

C.H. Lamborg<sup>a,\*</sup>, K.O. Buesseler<sup>a</sup>, J. Valdes<sup>a</sup>, C.H. Bertrand<sup>a</sup>, R. Bidigare<sup>b</sup>, S. Manganini<sup>a</sup>, S. Pike<sup>a</sup>, D. Steinberg<sup>c</sup>, T. Trull<sup>d</sup>, S. Wilson<sup>c</sup>

<sup>a</sup> Woods Hole Oceanographic Institution, Woods Hole, MA 02543, USA

<sup>b</sup> Department of Oceanography, University of Hawaii, Honolulu, HI 96822, USA

<sup>c</sup> Virginia Institute of Marine Science, College of William and Mary, Gloucester Point, VA 23062, USA

<sup>d</sup> Antarctic Climate and Ecosystems Cooperative Research Centre, University of Tasmania-CSIRO Marine and Atmospheric Research, Hobart 7001, Australia

## ARTICLE INFO

### Article history:

Accepted 11 April 2008  
Available online 7 May 2008

### Keywords:

Mesopelagic zone  
Sediment traps  
Sinking particles  
Organic carbon  
Nutrients  
Biominerals

## ABSTRACT

As part of the VERTIGO program, we collected and analyzed sinking particles using tethered and neutrally buoyant sediment traps at three depths in the oceanic mesopelagic zone and at two biogeochemically contrasting sites (N. Central Pacific at ALOHA; N. Pacific Western Subarctic Gyre at K2). This effort represented the first large-scale use of neutrally buoyant traps and represents a significant step forward in the study of the marine biological pump. In this paper, we present the results of mass, macronutrient, biominerals and phytoplankton pigment determinations made on these samples.

The impact of a variety of potential collection biases were examined, including those from in-trap particle degradation, zooplankton swimmers and poisons. Though these factors have been observed to affect results in other programs, we found them to have relatively little impact on measured fluxes in this study. There was evidence, however, that the neutrally buoyant traps performed better than the tethered traps in terms of flux accuracy during one deployment, possibly because of improved large particle collection efficiency.

Fluxes of material exhibited three different patterns through the mesopelagic: increasing, decreasing and constant with depth. Decreasing fluxes with depth were observed for all biogenic material formed in the euphotic zone. The attenuation of flux with depth was not the same for all components, however, with phytoplankton pigments exhibiting the greatest degradation with depth and particulate inorganic carbon the least. Organic carbon and nitrogen showed a very high correlation in these samples, with little evidence of different attenuation length scales. Increasing fluxes with depth were observed for particulate Ba at both sites and Al at K2. The increases in Ba are attributed to the formation of barite in degrading particles, while increasing Al at K2 was the result of lateral inputs from a continental shelf/slope. Constant fluxes with depth were observed for Al at ALOHA, where fluxes appeared to be in steady state with atmospheric dust deposition.

The mesopelagic zone at K2 was observed to attenuate particle flux less than at ALOHA, and with a higher POC/PIC (“rain”) ratio. These two factors combine to imply that the Subarctic province had a much more efficient biological pump than had the subtropical gyre during our occupations. This could be the result of either faster sinking particles, generated from grazing by large zooplankton, or inherently slower particle degradation rates.

© 2008 Elsevier Ltd. All rights reserved.

## 1. Introduction

With every stroke of the oceanic biological pump (e.g., Volk and Hoffert, 1985; Ho et al., 2003), particulate biogenic material is

formed in the surface ocean and sinks below the euphotic zone, driving mass and energy against the mixing force of mode water formation and thermohaline circulation. The functioning of the ocean's biological pump has been the subject of a great number of studies and was a central theme in the JGOFS program (e.g., Buesseler, 1998; Ducklow et al., 2001). Even with this scrutiny, there are a number of important features of how this pump works that bear further study. Of particular importance is

\* Corresponding author.

E-mail address: [clamborg@whoi.edu](mailto:clamborg@whoi.edu) (C.H. Lamborg).

the mesopelagic region (ca. from base of euphotic zone to 1000 m), where the majority of particle flux attenuation takes place. In some locations, this region of the water column is also above the permanent thermocline and therefore able to participate in annual biogeochemical recycling through deep winter mixing. Therefore, some material and energy recycled in the mesopelagic is still biogeochemically active on short timescales and directly diminishes the strength of the biological pump. Unfortunately, this segment of the oceanic water column has received relatively little attention in field programs due, in part, to the additional effort required to sample at these depths.

The goal of the *Vertical Transport In the Global Ocean* program (VERTIGO; Buesseler, Valdes, Siegel, Steinberg, PI's) was to study the inner workings of the biological pump in the marine mesopelagic zone through the collaborative, inter-disciplinary examination of the biology, chemistry and physics of two contrasting oceanic provinces (Buesseler et al., this volume). A major component of this effort has been the collection and analysis of sinking particles, and this report summarizes the elemental determinations made on these samples. From elemental analyses we can address not only the absolute magnitude of component fluxes associated with sinking particles but also issues related to the efficiency of the biological pump through determination of macronutrient ratios, the organic and inorganic carbon rain ratio, and the impact of biominerals on sinking rates and preservation of organic material. Furthermore, by measuring the flux of trace elements, we can examine the effects that the biological pump has on micronutrient recycling as well as in the cycling of particle-reactive elements in general. Such studies related to trace elements are particularly limited thus far (e.g., Knauer et al., 1984; Honjo and Manganini, 1993; Jickells et al., 1996; Kuss and Kremling, 1999; Pohl et al., 2004). The VERTIGO minor and trace flux element results are presented in a companion paper (Lamborg et al., this volume).

All of these VERTIGO flux measurements are ultimately designed to examine the mechanistic dependencies of the biological pump, and thereby search for connections between primary production, export and new production and the flux of material into the bathypelagic ocean. Hypotheses have been put forward to explain the cycling of organic and other material in surface waters as well as the bathypelagic, and which invoke a wide variety of controls including foodweb structure, temperature, and the presence of ballasting and/or protective biominerals (e.g., Michaels and Silver, 1988; Antia et al., 2001; Armstrong et al., 2002; François et al., 2002; Klaas and Archer, 2002; Lutz et al., 2002; Passow and De La Rocha, 2006).

An important part of studying particle flux in the mesopelagic zone is the development and application of new collection tools. Sediment traps of various kinds have been widely used to collect sinking particles but have many acknowledged limitations (e.g., Gardner, 2000; Buesseler et al., 2007a). Prominent among these are sampling inefficiencies and biases resulting from fluid shear across the mouth of the traps (e.g., Butman, 1986; Gust et al., 1994). This is a particular problem to sampling in the mesopelagic zone, which requires long tethering lines from either the surface or bottom, and horizontal currents and thus shear are generally higher than in the bathypelagic zone. Neutrally buoyant, "free vehicle" sampling devices are therefore very attractive for work at this depth, as they eliminate shear and tilt. In previous work, some of us have documented the development of a neutrally buoyant sediment trap (NBST), built around Argo float technology (Buesseler et al., 2000; Valdes and Price, 2000; Stanley et al., 2004). These devices are ballasted and programmed to sink to specified densities and maintain their position through passive and active measures. The VERTIGO program represents the first multi-instrument, multi-depth deployment of NBSTs and

therefore a significant advancement in our understanding of marine particle cycling.

## 2. Study sites

The two study sites for the VERTIGO program were located in the North Pacific Ocean (Buesseler et al., 2007b, this volume), at stations that are part of two time-series ocean observation programs. The first station occupied was ALOHA (22.75° N 158° W), located just north of the Hawaiian island of Oahu and the primary study location for the HOT program (<http://hahana.soest.hawaii.edu/hot>). ALOHA occupation took place from June 22 to July 8, 2004. The second site occupied, K2 (47° N 161° E), is part of time-series ocean observation program recently conducted by the Japanese Agency for Marine-Earth Science and Technology (JAMSTEC). K2 is located in the southwest corner of the Subarctic gyre of the northwest Pacific and our field work there was conducted between July 24 and August 16, 2005.

These two sites were chosen for the VERTIGO program because they represent two contrasting biogeochemical systems. ALOHA has been characterized as an oligotrophic, open-ocean gyre location, possessing warm surface waters and substantial cooling to a permanent thermocline at ca. 200 m (Bingham and Lukas, 1996). Though exhibiting relatively little seasonal variability in production, stock of phytoplankton and particle flux, the long-term observation of this ocean region has demonstrated slow, ongoing as well as more recent sudden shifts in system behavior, as characterized by changes in production and nutrient budgets (e.g., Karl et al., 2001a,b). The ALOHA primary producer community is dominated by small cells (*Prochlorococcus* and *Synechococcus*; e.g., Karl, 1999), though representatives of most phyla are to be found. In contrast, K2 is a location characterized by large seasonal variations in production, producer community (diatoms in summer and during our occupation) and flux. Deep winter convection gives rise to a sharp halo/pycnocline and temperature minimum feature at ca. 100 m, but the water column exhibits relatively uniform and cool temperatures (ca. 4 °C). Dissolved oxygen drops to very low (<50 μM) levels below the minimum halo/pycnocline and remains low through most of the mesopelagic zone. This appears to be the result of a combination of local oxygen consumption and advection from the Bering Sea shelf (e.g., Reid, 1997; Andreev and Kusakabe, 2001). Fig. 1 illustrates typical hydrography for both ALOHA and K2. A more detailed description of site conditions during our occupations can be found in Buesseler et al. (this volume).

## 3. Methods

### 3.1. Sediment trap systems

The fluxes of material reported here were measured using two kinds of sediment traps: conventional surface tethered traps ("Clap" Traps) and neutrally buoyant traps (NBSTs). Each Clap Trap consisted of a surface float (supporting a flasher, radar target and Argos/GPS transmitter), enough line to deploy a trap array to its target depth, a stainless steel rosette (capable of supporting 10 or more sediment trap tubes), an FSI current meter and finally a 5 m drogue. This array is analogous to the MultiPITS systems used extensively during JGOFS and still in use for measuring relatively shallow particle fluxes in programs such as HOT and BATS. One important difference between the Clap Traps and many of the MultiPITS of the past was the inclusion of the drogue at the end of the mooring, which was meant to help reduce hydrodynamic slip that can occur with surface tethered systems as a result of wind

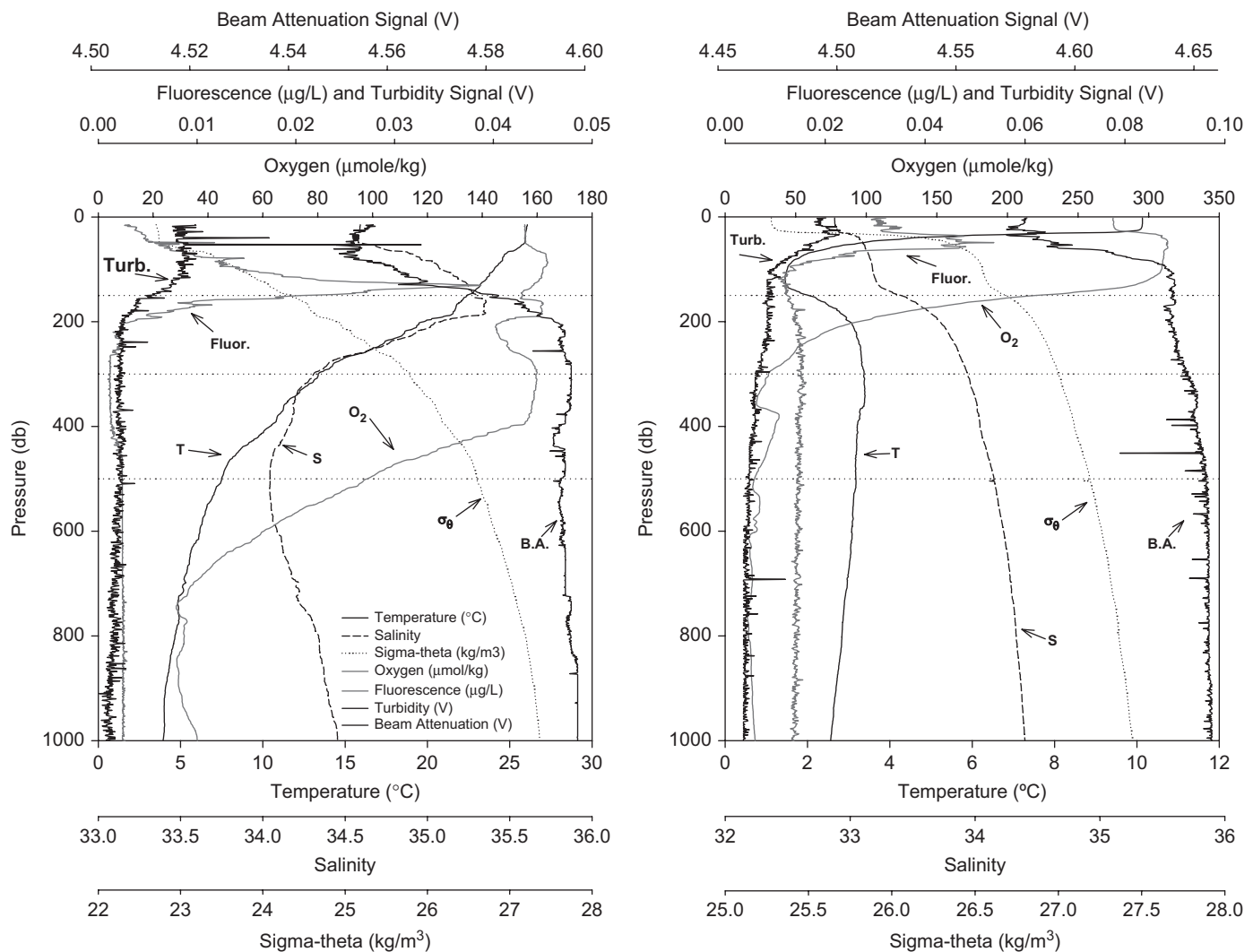


**Fig. 1.** Hydrography at the two VERTIGO sites. The dotted horizontal lines indicated the nominal depths of the sediment traps described in this work. Station ALOHA (left), has a warmer and more oxygenated mesopelagic zone (ca. 100–500 m) than does K2. Note different scaling on the x-axes between sites.

forcing. Such slip is thought to be one of the possible causes of problems with collection efficiency and sorting effects in sediment traps (Buesseler, 1991; Gust et al., 1996; Gardner, 2000). The attached current meters demonstrated that our Clap Trap rosettes did still move relative to the currents at depth (horizontal speeds were typically 0–10 cm s<sup>-1</sup>; see Section 4.1.4). The NBSTs minimize the issue of hydrodynamic slip altogether, by having no surface expression at all and are able to move with the ambient currents at depth and return to the surface for recovery following a predetermined, programmable amount of time.

Both trapping systems were deployed with identical sediment trap tubes (diameter 12.7 cm; length 70 cm) that consisted of a polycarbonate tube body, a HDPE tube lid, honeycomb screen (hole size ca. 1 cm diameter) and HDPE tube base. The base was a shallow cone that terminated in a valve with a 0.5 cm diameter orifice (Cole-Parmer). The tube lid was held in place by a length of amber silicone shock cord and the honeycomb screen was fixed at 2.5 cm below the mouth of the tube to accommodate the lid when closed. Each tube lid also had a nylon lanyard that was looped over a withdrawing pin mechanism, contained in a pressure casing located either in the middle of the Clap Trap rosette, or part of the NBST main body. During deployment of the trapping systems, the pin held each tube lid in the open position, against the tension of

their shock cords. Just prior to recovery, the pin mechanism was programmed to withdraw into its housing, releasing the lids to their closed position. Thus, the traps were deployed open, but retrieved closed to better preserve sample integrity during recovery. Sediment traps were deployed twice during each site occupation, and the systems remained in the water between 3 and 5 days (Table 1). For each deployment, the traps were released in as rapid a succession as possible, over the course of about 12 h. The start dates for the two deployments at each site were about 11 days apart.

### 3.2. Trap tube handling, deployment and recovery

The assembled trap tubes were cleaned prior to use in three steps: 2 day soak in a 5% detergent (Micro) solution, 1 week soak in 1% HCl and 1 week soak in 1% HNO<sub>3</sub>. After each solution, the tubes were thoroughly washed with 18 MΩ cm<sup>-1</sup> water, then were double bagged for transport to the field. At sea, prior to their first use, they were soaked for more than 48 h in 0.2 µm filtered seawater (500 m). Just prior to deployment, the tubes were filled with 0.2 µm filtered water from the depth to which they were to be deployed. Then 500 mL of a borate-buffered brine ( $S > 70$ ; 3 mM borate, pH = 8) solution, formed from freeze-concentrating

**Table 1**

Description of the depth and durations of sediment trap deployments

System	Nominal depth (m)	ALOHA deployment duration (1st/2nd deployment; days)	K2 deployment duration (1st/2nd deployment; days)
NBST 13	150	2.60/3.04	3.20/3.35
NBST 15	150	2.63/3.16	3.21/3.33
NBST 17	150	2.65/3.13	3.18/3.32
NBST 14	300	3.38/3.79	4.24/4.22
NBST 16	300	3.40/3.83	4.26/4.21
NBST 11	500	4.29/4.71	0.94 <sup>a</sup> /5.13
NBST 12	500	4.33/4.75	4.94/3.88 <sup>a</sup>
Clap Trap 1	150	3.07/3.23	3.25/3.36
Clap Trap 2	300	3.86/4.11	4.23/4.29
Clap Trap 3	500	4.78/4.98	4.99/5.18

NBST = neutrally buoyant sediment trap; Clap Trap = surface-tethered trap.

<sup>a</sup> These two NBSTS aborted their missions early.

0.2 µm filtered Sargasso seawater (400 m), was dispensed into the bottom of the tube by slowly pouring the brine down a acid-washed Teflon tube. The brine was also poisoned with either formalin or Hg at concentrations recommended to retard bacterial activity (37 mM and 180 µM, respectively; Lee et al., 1992; Hedges et al., 1993). In most instances, the brine layer was still intact upon recovery of systems as indicated by visual inspection.

During the trap deployments, replicate NBSTS were deployed (3 at 150 m, 2 each at 300 and 500 m). Each NBST carried on it 5 sediment trap tubes, 4 used for biogeochemical measurements (2 poisoned with formalin and 2 with Hg) and a fifth, preserved with formalin, that was dedicated for biological identification. One Clap Trap array was deployed per target depth and each carried 10 tubes. Five of these were processed identically to those on board the NBSTS, 1 was a covered process blank, 2 were used for in-trap material aging experiments (see below) and 2 supported the "Gel Traps" prepared by the University of Tasmania group. Surface drift tracks for the CLAP traps and deployment and recovery positions for NBSTS can be found in Buesseler et al. (this volume; Fig. 7 therein).

Upon recovery of the traps, the tubes were removed from their support/vehicle, and allowed to stand for at least 1 h so that in-tube material could finish sinking into the brine. Then all but ca. 1 L of fluid was pumped out of top of the tubes, and the remaining liter of fluid/sediment mixture was collected into a 4 L, acid-washed fluorinated HDPE bottle. A small rinse of the tube using depth relevant filtered seawater was also made and collected along with the sample. During the collection, the water/particle mixture was passed through an acid-washed nylon mesh (350 µm pore), in a Teflon filter holder (Savillex) to remove most zooplankton "swimmers." When possible, two tubes of like poison were pooled together. Pooling was not done with the covered process blank or when tubes were deemed to be anomalous (e.g., did not close). When done, pooling simply involved the collection of water/particle mixtures from two tubes in the same 4 L bottle and through the same screen. After sample collection and any pooling, the Teflon filter housing was opened and the screen rinsed with the appropriate filtered seawater and saved for microscopic examination.

### 3.3. Sample splitting

Once the water/sediment mixtures were collected, they were immediately wet split into 8 equal fractions. This was done by means of a custom splitter device operated within a HEPA-filtering laminar flow bench. The splitter is illustrated in Fig. 2,



**Fig. 2.** Photograph of the custom wet splitting device used to generate equivalent subsamples of sediment trap material for a variety of analyses. Built for Café Thorium by Rich Zuck.

and consists of a PVC base and top plate, a Lucite rotating dispenser cap and fill tube. The basic operation involved pouring the water/particle mixture into the cap as it was rotating. The fluid then moved through the cap and out through a drain that passed over funnels in the top plate that fed into the split bottles. Hands-free delivery of the samples was made possible by attaching a custom nozzle fitting to the 4 L bottle, which fed to the splitter via a  $\frac{1}{4}$ " Teflon tube. The bottle was gently swirled to get the water/particle mixture moving, and then inverted and set on stand that was bolted to an orbital shaker that was higher than the splitter. The shaker was then started and kept the bottle contents slowly moving. We had a Teflon stopcock in-line just above the splitter to allow flow of water/particle to be controlled, but found it more effective to start with the splitter already operating and the valve open so that the material could be allowed to start draining out immediately. After the initial drain/split of the sample, the walls of the bottle were washed down with a small amount of filtered, depth appropriate seawater and this wash split as well.

We found the splitter effectiveness for equal distribution of samples of water to be excellent (splits were within <1% of each other in fluid mass) and of particles to be very good as well (one test found splits agreed in their  $^{234}\text{Th}$  activity within 3%;

$n = 5$ ). In some cases (noted below), the same kind of analysis (mass, carbon,  $^{234}\text{Th}$ ) was done on separate splits, and this precision was often good as well (agreement to within 15%). Thus, pooling of multiple tubes and subsequent splitting allowed nearly identical subsamples, destined for different measurements, to be generated. This removes the unavoidable tube-to-tube variability that adds noise to data sets when separate tubes are used for different analyses, such as is common among many PITS-based sampling programs, such as at the US time-series Programs (BATS and HOT).

### 3.4. Sample replication, processing and analysis

Typical replication can be summarized as two samples from each device, with 3–4 devices per depth, and 1 or 2 determinations (e.g., for mass) per sample, or a total of 6–16 determinations per depth. Recent statistical analysis of flux modeling has suggested that replicate determinations of flux properties is the best way to help constrain the models of flux in the ocean (Primeau, 2006).

The sample splits were processed in different ways to accommodate a variety of determinations (Table 2). All sample processing took place immediately after splitting in a HEPA air filtered flow bench (Micron-Aire and Ray Products) and observing clean techniques (acid-washed plastic funnels, forceps, Petri dishes and handling with gloved hands, double bagging of samples and processware, etc.). The elemental, biomineral and pigment determinations made on the sediment trap material are reported here. Additional analyses (including fecal pellet characterization) are reported elsewhere in this issue (Wilson et al., this volume).

#### 3.4.1. Mass

The mass flux collected in the sediment trap was determined gravimetrically on two of the sample splits, both filtered onto polycarbonate membranes (Nuclepore; 1  $\mu\text{m}$  nominal pore size). Prior to use, the filters were acid-washed by soaking in 1% HCl and 1%  $\text{HNO}_3$  for at least 1 week each, rinsing and drying in a laminar flow bench. The filters were further dried by holding them in a silica gel desiccators for 2 days. Following the drying period, the filters were weighed to the nearest  $\mu\text{g}$  on a Mettler AT21 Comparator.

Following the splitting of the samples at sea, these filters were rinsed with a small amount of borate-buffered  $18 \text{ M}\Omega \text{ cm}^{-1}$  water. Upon return to the lab following collection, the samples were again desiccated and weighed multiple times to a constant weight. During weighing, the filters were handled cleanly so that element analyses could be performed on the same filters. In

addition to the covered process tube blanks, unused filters were reweighed as lab blanks.

#### 3.4.2. Carbon and nitrogen

Total sinking particulate carbon and nitrogen were determined using a high-temperature combustion technique on a Thermo Electron FlashEA 1112 C/N analyzer. This analysis was performed on subsamples (determined gravimetrically) of the splits filtered onto Ag membrane filters (Sterlitech; nominal pore size 1.2  $\mu\text{m}$ ).

#### 3.4.3. $^{234}\text{Th}$

The activity of  $^{234}\text{Th}$  associated with sinking particles was determined on sample splits filtered on Ag filters. Filters were not rinsed following filtering but allowed to dry in the flow bench. The filters were covered with a Mylar/foil layer and counted at sea for total high energy beta activity using a low background, anti-coincidence detector (Risø National Laboratories) at sea and again at 6 months following collection (e.g., Buesseler et al., 2005; van der Looff et al., 2006). This allows characterization of the overall decay of the total beta signal as well as the establishment of non- $^{234}\text{Th}$ -associated beta background in the samples.

#### 3.4.4. Particulate inorganic carbon

This analysis was also carried out on rinsed polycarbonate filters, as with mass (Section 3.4.1). Carbonate in the sediment trap samples was determined by coulometric carbon analysis of  $\text{CO}_2$  evolved from sample aliquots acidified with phosphoric acid (e.g., Johnson et al., 1985; Honjo et al., 2000).

#### 3.4.5. Particulate organic carbon

The amount of particulate organic carbon was determined by subtracting the particulate inorganic carbon from the total carbon.

#### 3.4.6. Biogenic silica

Total silica was determined on aliquots of Ag filters using a Lachat QuikChem FIA+autoanalyzer and standard methods (e.g., Muller and Schneider, 1993). The filter aliquot was first digested in weak base, and thus the total silica determined in the extract was comprised of only biogenic silica.

#### 3.4.7. Phosphorus and selected metals

These elements were determined by magnetic sector inductively coupled plasma mass spectrometry (ICPMS), performed on the same splits as for mass (acid-washed polycarbonate). The methods used here were similar to those used during preliminary NBST development (Stanley et al., 2004). In brief, aliquots were cut from the whole filter using ceramic scissors and the sample

**Table 2**

Summary of the processing and analyses performed on the various at-sea splits of sediment trap material during VERTIGO

Split	Filter type	Treatment	CHN	bSi	ICPMS	$^{234}\text{Th}?$	Mass?	PIC	Other/archive <sup>a</sup>
a	Ag	Dry	0.5	0.25		y <sup>b</sup>			0.25
b	Nucl	Rinse and dry <sup>c</sup>			1		y <sup>b</sup>		
c	QMA	L-N <sub>2</sub>							1
d	Ag	Pick and dry <sup>d</sup>	0.5	0.25		y			0.25
e	Ag	Dry				y			1
f	Nucl	Rinse and dry					y	1	
g	Ag <sup>e</sup>	Freeze							1
h	QMA	Freeze							1

The split label is the arbitrary identifier given to each split and along with the "V#" comprises a unique split sample identifier.

<sup>a</sup> Other/archive denotes analyses that are not reported here.

<sup>b</sup> y means that the non-destructive analysis of either  $^{234}\text{Th}$  or total mass was completed on these fractions sometimes in addition to other determinations.

<sup>c</sup> Rinse and dry means small rinse with buffered  $18 \text{ M}\Omega \text{ cm}^{-1}$  following filtration (see Section 3.4.1).

<sup>d</sup> Pick and dry processing was done on the d fraction only and included manual removal of zooplankton from the water/particle mixture prior to filtration.

<sup>e</sup> These Ag filters were pre-combusted.

fraction determined gravimetrically. The aliquots were then digested in a hot block (120 °C) for >4 h in small sealed Teflon vials (Savillex). The digestion solution was a 5 mL 4:1 mixture of concentrated trace metal grade HNO<sub>3</sub> and HF. Some samples were also pre-digested with 0.2 mL of concentrated NH<sub>4</sub>OH to aid in filter digestion, but results suggested that incomplete digestion of the filter matrix made little difference to the results (Lamborg et al., this volume). Following cooling of the sample, 0.1 mL of saturated boric acid solution was made to aid in dissolution of CaF<sub>2</sub> (e.g., Collier, 1991). The concentrated samples were held until analysis in acid-washed LDPE vials. Prior to analysis, the concentrated digest was quantitatively diluted to ca. 20× in a 5% 4:1 HNO<sub>3</sub>:HF, spiked to ca. 0.5 ppm with <sup>115</sup>In. The In-spiked diluent was made in bulk so that all samples analyzed during a single day would be diluted with a solution containing identical In concentrations. A similar digestion approach was recently compared to a borate fusion method, and found to agree well for most elements (Huang et al., 2007).

The diluted samples were analyzed on a Thermo Electron Finnigan Element 2, outfitted with an Aridus desolvating nebulizer and ASX-100 autosampler (both CETAC), with sample take up rates at 0.1 mL min<sup>-1</sup>. <sup>114</sup>Cd, <sup>115</sup>In, <sup>137</sup>Ba and <sup>208</sup>Pb were measured in low resolution ( $\Delta = 300$ ) with 20 scans while <sup>23</sup>Na, <sup>25</sup>Mg, <sup>27</sup>Al, <sup>31</sup>P, <sup>44</sup>Ca, <sup>45</sup>Sc, <sup>47</sup>Ti, <sup>51</sup>V, <sup>55</sup>Mn, <sup>56</sup>Fe, <sup>59</sup>Co, <sup>60</sup>Ni, <sup>63</sup>Cu, <sup>66</sup>Zn and <sup>88</sup>Sr were measured in medium resolution ( $\Delta = 4000$ ) for 5 scans.

Four different SRMs were processed and analyzed by ICPMS as well (at least two in any given analysis session), including NIST 1573a (Tomato Leaves), NRC HISS-1 and MESS-3 and USGS MAG-1. Results agreed with certified values within 10% in most cases, except for MESS-3, which was not always completely digested by this approach. The ICPMS results for P, Na, Al, Sr, Ba and Ca are included in this manuscript, while those for the others are included in a companion paper (Lamborg et al., this volume).

#### 3.4.8. Phytoplankton pigments

Phytoplankton pigments were determined on sediment trap material subsamples stored in liquid nitrogen until analysis, using HPLC methods (Bidigare et al., 1985; Wright et al., 1991).

#### 3.4.9. Process blanks

As noted, the covered tube on board the Clap Trap array was used as a process blank, and subjected to all the same processing protocols as the samples. The blank "fluxes" are included in Table 3 for comparison to the samples and are calculated by dividing the average blank value for each parameter by a nominal deployment time of 4 days. While most samples were well above their respective detection limits, the process blanks often represented non-trivial fractions of the sample. Sodium found in the sediment trap material was assumed to be the result of retention of seawater salt, and was therefore used to correct element fluxes for this artifact. The only elements that were found to require a seawater salt correction were Mg and Ca, with almost all the Mg appearing to be salt derived. The Ca seasalt corrections were generally less than 1%.

## 4. Results and discussion

### 4.1. Sediment trap methodological issues

#### 4.1.1. In-trap solubilization experiments

Though the traps were poisoned/preserved/buffered, we were concerned that some degradation of collected particles could occur before recovery and processing of the samples. Such an

issue has been suggested to significantly lower estimated fluxes of material, especially in moored traps that are deployed for long periods of time (e.g., Noji et al., 1999; Kahler and Bauerfeind, 2001; Antia, 2005). To address this, we selected two of the tubes on the Clap Traps to be combined and used the splits as individual time points in aging experiments (standard poisoned tubes). To do this, the splits were held in the dark and at temperatures representative of the depths from which they came (i.e., 25, 15 and 5 °C for 150, 300 and 500 m at ALOHA and 4 °C at K2). The splits were sacrificed at specific times (1, 2, 3 and 5 days after collection) by filtering as noted in Section 3, and the same range of analyses were performed. In addition, during the ALOHA occupation, subsamples for DOC were collected from the overlying fluid of the Hg preserved samples. Results from a few of the determinations made on ALOHA material are shown in Fig. 3, and in the case of the particulate components, are shown normalized to Al to account for variations in particle loading. The impact of in-trap particle degradation on the accurate determination of flux can be assessed from these experiments by fitting the Al-normalized aging curves with an exponential function and using the fitted pseudo-first-order rate constant in the time rate of change equation for collected material:

$$\frac{dx}{dt} = F - kx \Rightarrow F = \frac{kx_t}{(1 - e^{-kt})}$$

where  $x$  is the amount of a component or element in the sediment trap,  $F$  is the flux of material into the trap (amount day<sup>-1</sup>) and  $k$  is the in-trap degradation rate constant measured in the aging experiments. The apparent flux is simply the amount  $x$  found at the end of the deployment divided by the deployment time. The ratio of the true flux (as described by  $F$  in the equation above) by the apparent flux is equal to

$$R_F = \frac{kt}{(1 - e^{-kt})}$$

None of the K2 aging experiments yielded significant loss of particulate material over 5 days. For the ALOHA samples, a few treatments exhibited  $k$  values that were significantly different from 0, and of these most suggested flux corrections on the order of 10%. The exceptions are shown in Table 4, and ranged from corrections of 14–48% for P, Ba, Mn, Fe and Sr at ALOHA, and are not necessarily associated with one poison or the other (Hg-deployment 1; formalin-deployment 2). For the minor and trace elements, these errors are comparable to the uncertainties observed between duplicate flux determinations and are not consistent within elements and deployments. Thus, even as there was evidence for some loss of material from the collected particles under some conditions, we have made no attempt to correct our measured fluxes as a result. In general, however, we can say that no measurable degradation occurred at K2 and relatively little degradation of material occurred at ALOHA, with some evidence in more than one sample for particulate P, Ba and Sr losses prior to our recovery of the devices. It should be noted that this site-to-site difference in degradation was mirrored in incubations conducted on unpoisoned material as well (not shown), suggesting that K2 material was inherently less degradable.

The relative lack of in-trap solubilization observed in VERTIGO samples differs from the conclusions in Antia (2005), who compiled data on P loss to the trap supernatant (and C, N and Si) and found much larger losses of P, >80%, in her shallowest data from 500 m (comparing initial and final supernatant concentrations). The main difference is that these high particulate P losses were from time-series moored traps with 1-year deployment times. Similarly, a 6 month time-series deployment for depths <600 m in the Cariaco, measured 20–40% P losses in the trap supernatant (O'Neill et al., 2005). In comparing these

**Table 3**  
Flux summaries for both sites

Site/deployment	Device	Depth (m)	Mass ( $\text{mg m}^{-2} \text{d}^{-1}$ )	TC ( $\text{mmole m}^{-2} \text{d}^{-1}$ )	N ( $\text{mmole m}^{-2} \text{d}^{-1}$ )	P ( $\mu\text{mole m}^{-2} \text{d}^{-1}$ )	POC ( $\mu\text{mole m}^{-2} \text{d}^{-1}$ )	bSi ( $\mu\text{mole m}^{-2} \text{d}^{-1}$ )	$^{234}\text{Th}$ ( $\text{dpm m}^{-2} \text{d}^{-1}$ )
<b>(a)</b>									
ALOHA, 1st	NBST 13	150	n/a	1.57 ± 0.25	0.20 ± 0.02	n/a	n/a	127 ± 73	227 ± 23
ALOHA, 1st	NBST 15	150	69 ± 9	1.62 ± 0.21	0.18 ± 0.03	5.4 ± 0.7	88.4 ± 0.6	1.53 ± 0.25	66 ± 3
ALOHA, 1st	NBST 17	150	51 ± 6	1.45 ± 0.38	0.18 ± 0.07	4.5 ± 3.2	62.9 ± n/a	1.39 ± 0.43	54 ± 17
ALOHA, 1st	NBST 14	300	30 ± 14	0.67 ± 0.17	0.07 ± 0.02	1.5 ± 0.9	60.6 ± n/a	0.61 ± 0.20	45 ± 20
ALOHA, 1st	NBST 16	300	29 ± 3	0.62 ± 0.07	0.05 ± 0.01	1.9 ± 0.9	87.4 ± n/a	0.54 ± 0.03	49 ± 1
ALOHA, 1st	NBST 11	500	13 ± 8	0.41 ± 0.11	0.03 ± 0.01	0.9 ± n/a	31.6 ± n/a	0.37 ± 0.05	32 ± 3
ALOHA, 1st	NBST 12	500	17 ± 3	0.36 ± 0.01	0.02 ± 0.00	3.6 ± n/a	68.1 ± n/a	0.29 ± 0.01	39 ± 16
ALOHA, 1st	Clap Trap	150	73 ± 3	1.83 ± 0.37	0.21 ± 0.05	4.4 ± n/a	n/a	n/a	72 ± 29
ALOHA, 1st	Clap Trap	300	37 ± 5	0.79 ± 0.05	0.07 ± 0.01	3.1 ± 1.9	139.5 ± n/a	0.65 ± 0.02	74 ± 5
ALOHA, 1st	Clap Trap	500	29 ± 2	0.65 ± 0.16	0.06 ± 0.02	1.9 ± 0.2	80.9 ± n/a	0.57 ± 0.09	45 ± 11
ALOHA, 2nd	NBST 13	150	61 ± 5	1.37 ± 0.08	0.15 ± 0.01	4.4 ± 1.3	91.1 ± n/a	1.28 ± 0.08	n/a
ALOHA, 2nd	NBST 15	150	50 ± 3	1.43 ± 0.04	0.16 ± 0.01	3.3 ± 1.3	78.1 ± 0.1	1.35 ± 0.02	71 ± n/a
ALOHA, 2nd	NBST 17	150	80 ± 27	1.94 ± 0.62	0.23 ± 0.07	7.8 ± 2.3	85.0 ± n/a	1.86 ± 0.71	90 ± 19
ALOHA, 2nd	NBST 14	300	29 ± 3	0.76 ± 0.13	0.08 ± 0.02	2.6 ± 0.5	73.4 ± n/a	0.65 ± 0.16	48 ± n/a
ALOHA, 2nd	NBST 16	300	29 ± 2	0.49 ± 0.11	0.06 ± 0.00	2.5 ± 1.6	90.2 ± n/a	0.40 ± 0.07	42 ± 5
ALOHA, 2nd	NBST 11	500	18 ± 1	0.37 ± 0.10	0.03 ± 0.01	0.8 ± 0.3	57.7 ± n/a	0.31 ± 0.08	47 ± 6
ALOHA, 2nd	NBST 12	500	17 ± 9	0.39 ± 0.20	0.05 ± 0.00	1.6 ± n/a	n/a	n/a	220 ± 30
ALOHA, 2nd	Clap Trap	150	65 ± 8	1.32 ± 0.38	0.15 ± 0.05	5.9 ± 2.1	143.9 ± n/a	1.11 ± 0.30	117 ± n/a
ALOHA, 2nd	Clap Trap	300	43 ± 6	0.84 ± 0.09	0.07 ± 0.01	2.9 ± 0.9	132.8 ± n/a	0.71 ± 0.07	66 ± 14
ALOHA, 2nd	Clap Trap	500	25 ± 3	0.50 ± 0.05	0.04 ± 0.01	2.1 ± 0.6	108.8 ± n/a	0.39 ± 0.02	47 ± 15
ALOHA	Blik <sup>a</sup>	150	8 ± 2	0.11 ± 0.04	0.005 ± 0.005	<20	~0.11 ± 0.04	4 ± 2	0 ± 43
HOT avg <sup>b</sup>	MultiPITS	150	63 ± 24	2.41 ± 0.82	0.31 ± 0.11	11 ± 5	250 ± 133	n/a	89 ± 64
HOT June '04 <sup>b</sup>	MultiPITS	150	n/a	2.84	0.39	11	241	n/a	88
HOT Aug '04 <sup>b</sup>	MultiPITS	150	n/a	1.97	0.21	3.9	n/a	n/a	283
<b>(b)</b>									
Site/deployment	Device	Depth (m)	Ba ( $\mu\text{g m}^{-2} \text{d}^{-1}$ )	Al ( $\mu\text{g m}^{-2} \text{d}^{-1}$ )	Ca ( $\mu\text{g m}^{-2} \text{d}^{-1}$ )	Sr ( $\mu\text{g m}^{-2} \text{d}^{-1}$ )			
ALOHA, 1st	NBST 13	150	n/a	n/a	n/a	n/a			
ALOHA, 1st	NBST 15	150	33.2 ± 8.2	466 ± 70	7862 ± 1338	152 ± 20			
ALOHA, 1st	NBST 17	150	28.7 ± n/a	280 ± 105	4714 ± 391	141 ± 76			
ALOHA, 1st	NBST 14	300	26.2 ± n/a	235 ± 211	5364 ± 2006	80 ± 30			
ALOHA, 1st	NBST 16	300	20.3 ± 3.6	451 ± 229	5723 ± 716	60 ± 10			
ALOHA, 1st	NBST 11	500	13.5 ± 3.1	158 ± 71	3161 ± 1690	27 ± n/a			
ALOHA, 1st	NBST 12	500	19.9 ± 6.2	230 ± 167	3912 ± 1800	26 ± 17			
ALOHA, 1st	Clap Trap	150	16.9 ± n/a	288 ± n/a	9381 ± n/a	174 ± n/a			
ALOHA, 1st	Clap Trap	300	29.2 ± 1.5	457 ± 96	9791 ± 1058	74 ± 3			
ALOHA, 1st	Clap Trap	500	33.7 ± 3.5	372 ± 147	5225 ± 480	36 ± 2			
ALOHA, 2nd	NBST 13	150	11.8 ± 0.2	191 ± 26	4584 ± 1898	168 ± 3			
ALOHA, 2nd	NBST 15	150	6.9 ± 4.5	139 ± n/a	4060 ± 2877	227 ± n/a			
ALOHA, 2nd	NBST 17	150	19.1 ± 7.8	132 ± 99	6590 ± 209	353 ± 44			
ALOHA, 2nd	NBST 14	300	13.6 ± 2.4	110 ± 15	3695 ± 458	110 ± 29			
ALOHA, 2nd	NBST 16	300	14.2 ± 2.1	139 ± 7	4555 ± 2069	59 ± 28			
ALOHA, 2nd	NBST 11	500	16.5 ± 1.3	112 ± 26	3739 ± 712	97 ± n/a			
ALOHA, 2nd	NBST 12	500	22.3 ± n/a	279 ± n/a	5069 ± n/a	46 ± n/a			
ALOHA, 2nd	Clap Trap	150	12.2 ± 6.6	152 ± 127	6459 ± 4150	150 ± 146			
ALOHA, 2nd	Clap Trap	300	30.2 ± 1.9	364 ± 56	7078 ± 408	92 ± 8			
ALOHA, 2nd	Clap Trap	500	38.0 ± 8.5	334 ± 53	6830 ± 495	75 ± 4			
ALOHA	Blik <sup>a</sup>	All	0.4 ± 0.2	12 ± 2	146 ± 186	3 ± 4			
HOT avg <sup>b</sup>	MultiPITS	150	n/a	n/a	n/a	n/a			
HOT Jun '04 <sup>b</sup>	MultiPITS	150	n/a	n/a	n/a	n/a			
HOT Aug '04 <sup>b</sup>	MultiPITS	150	n/a	n/a	n/a	n/a			

(c)																	
Site/deployment	Device	Depth (m)	CHL c	Per	But	Fuco	Hex	Viola	DDX	Lut	Zeax	MV-CHL b	$\alpha$ -CAR	$\beta$ -CAR	DV-CHL a	MV-CHL a	Tot. CHL a
ALOHA, 1st	NBST 13	150	n/a	n/a	n/a	n/a	n/a	n/a	n/a	n/a	n/a	n/a	n/a	n/a	n/a	n/a	
ALOHA, 1st	NBST 15	150	1.46 ± 0.63	1.65 ± 0.38	4.18 ± 0.79	1.73 ± 0.28	11.25 ± 0.06	0.43 ± 0.26	0.64 ± 0.08	0.00	6.02 ± 0.97	9.13 ± 1.33	6.45 ± 1.40	1.28 ± 0.46	4.41 ± 0.37	12.30 ± 0.43	16.29 ± 0.81
ALOHA, 1st	NBST 17	150	1.83 ± 0.27	1.48 ± 0.47	3.90 ± 1.04	1.71 ± 0.48	10.04 ± 1.66	0.39 ± 0.55	0.82 ± 0.06	0.26 ± 0.37	5.80 ± 0.27	8.31 ± 0.73	5.28 ± 1.00	1.08 ± 0.29	3.50 ± 0.26	12.80 ± 1.86	16.29 ± 2.11
ALOHA, 1st	NBST 14	300	0.00	0.00	0.00	0.50 ± 0.08	2.24 ± 0.23	0.00 ± 0.00	0.00 ± 0.00	0.00	2.51 ± 0.13	3.02 ± 0.40	1.86 ± 0.20	0.30 ± 0.10	1.82 ± 0.39	1.35 ± 0.05	3.17 ± 0.33
ALOHA, 1st	NBST 16	300	0.00	0.00	0.28 ± 0.08	0.40 ± 0.22	2.66 ± 0.70	0.33 ± 0.17	0.00 ± 0.00	0.00	2.86 ± 0.52	3.45 ± 0.17	2.25 ± 0.16	0.67 ± 0.31	1.87 ± 0.22	2.61 ± 1.94	4.48 ± 2.16
ALOHA, 1st	NBST 11	500	0.00	0.00	0.00	0.14 ± 0.20	0.64 ± 0.08	0.00	0.00 ± 0.00	0.00	1.22 ± 0.04	2.79 ± 1.19	0.90 ± 0.02	0.22 ± 0.03	0.82 ± 0.10	1.23 ± 0.08	2.05 ± 0.18
ALOHA, 1st	NBST 12	500	0.00	0.00	0.00	0.00 ± 0.00	0.00 ± 0.00	0.00	0.00 ± 0.00	0.00	0.93 ± 0.08	0.79 ± 1.11	0.72 ± 0.01	0.00 ± 0.00	1.21 ± 0.36	0.26 ± 0.15	1.47 ± 0.21
ALOHA, 1st	Clap Trap	150	2.96 ± 0.00	1.81 ± 0.00	4.51 ± 0.00	1.68 ± 0.00	13.52 ± 0.00	0.80 ± 0.00	0.84 ± 0.00	0.42 ± 0.00	8.54 ± 0.00	10.42 ± 0.00	8.72 ± 0.00	1.53 ± 0.00	5.64 ± 0.00	11.49 ± 0.00	17.13 ± 0.00
ALOHA, 1st	Clap Trap	300	0.00	0.00	0.32 ± 0.45	0.64 ± 0.32	2.35 ± 0.29	0.59 ± 0.25	0.10 ± 0.14	0.00	3.15 ± 0.29	3.86 ± 1.03	2.88 ± 0.51	0.49 ± 0.05	2.66 ± 0.15	0.04 ± 0.06	2.70 ± 0.09
ALOHA, 1st	Clap Trap	500	0.00	0.00	0.00	0.14 ± 0.20	1.38 ± 0.36	0.00	0.00 ± 0.00	0.00	1.90 ± 0.36	2.28 ± 0.59	1.51 ± 0.08	0.34 ± 0.08	1.52 ± 0.46	0.61 ± 0.73	2.12 ± 0.27
ALOHA, 2nd	NBST 13	150	2.54 ± 0.49	0.90 ± 1.27	2.29 ± 2.84	1.58 ± 1.61	6.60 ± 6.90	0.83 ± 0.48	0.58 ± 0.56	0.32 ± 0.45	5.52 ± 4.92	3.95 ± 2.51	4.35 ± 3.86	1.09 ± 0.72	1.67 ± 0.32	9.81 ± 10.56	11.49 ± 10.88
ALOHA, 2nd	NBST 15	150	2.25 ± 0.20	1.96 ± 0.51	4.46 ± 0.84	2.05 ± 0.07	12.67 ± 0.05	0.93 ± 0.11	0.66 ± 0.05	0.65 ± 0.01	8.82 ± 1.06	9.12 ± 1.71	8.07 ± 0.38	1.50 ± 0.18	4.44 ± 0.24	12.98 ± 3.01	17.41 ± 3.24
ALOHA, 2nd	NBST 17	150	2.49 ± 0.93	1.85 ± 0.59	3.94 ± 0.22	2.09 ± 0.55	11.13 ± 0.26	0.82 ± 0.17	0.88 ± 0.50	0.31 ± 0.44	5.73 ± 1.14	8.83 ± 0.67	6.49 ± 0.70	1.31 ± 0.34	1.36 ± 0.50	14.79 ± 2.60	16.15 ± 2.11
ALOHA, 2nd	NBST 14	300	0.25 ± 0.17	1.25 ± 1.28	2.13 ± 2.25	1.91 ± 1.19	5.99 ± 4.74	1.19 ± 1.18	0.61 ± 0.46	0.00	6.16 ± 5.03	4.66 ± 1.34	4.58 ± 3.63	1.34 ± 0.52	1.89 ± 0.37	10.92 ± 10.49	12.81 ± 10.13
ALOHA, 2nd	NBST 16	300	0.09 ± 0.12	0.00	0.20 ± 0.28	0.61 ± 0.35	2.35 ± 0.09	0.36 ± 0.00	0.00 ± 0.00	0.00	2.30 ± 0.46	3.61 ± 0.81	1.83 ± 0.19	0.55 ± 0.03	1.50 ± 0.10	2.20 ± 0.89	3.70 ± 0.99
ALOHA, 2nd	NBST 11	500	0.11 ± 0.01	0.00	0.00	0.66 ± 0.01	1.09 ± 0.36	0.08 ± 0.11	0.12 ± 0.07	0.00	1.33 ± 0.06	1.39 ± 0.45	0.68 ± 0.35	0.58 ± 0.04	0.64 ± 0.31	3.63 ± 0.25	4.27 ± 0.06
ALOHA, 2nd	NBST 12	500	0.14 ± 0.00	0.00	0.00	0.48 ± 0.00	1.15 ± 0.00	0.21 ± 0.00	0.00 ± 0.00	0.00	1.83 ± 0.00	3.09 ± 0.00	1.28 ± 0.00	0.46 ± 0.00	1.11 ± 0.00	2.52 ± 0.00	3.63 ± 0.00
ALOHA, 2nd	Clap Trap	150	1.61 ± 0.12	1.57 ± 0.41	3.71 ± 0.64	2.08 ± 1.04	9.87 ± 2.03	0.81 ± 0.47	0.56 ± 0.28	0.33 ± 0.15	6.06 ± 1.14	6.13 ± 1.05	6.19 ± 0.49	1.28 ± 0.23	3.22 ± 1.27	9.89 ± 3.91	13.11 ± 2.64
ALOHA, 2nd	Clap Trap	300	0.18 ± 0.25	0.20 ± 0.28	0.21 ± 0.30	1.04 ± 0.22	2.36 ± 0.10	0.69 ± 0.02	0.13 ± 0.18	0.21 ± 0.30	3.26 ± 0.33	3.92 ± 0.30	2.56 ± 0.12	0.84 ± 0.03	2.45 ± 0.30	2.35 ± 0.16	4.80 ± 0.14
ALOHA, 2nd	Clap Trap	500	0.01 ± 0.02	0.00	0.00	0.60 ± 0.11	0.93 ± 0.28	0.15 ± 0.02	0.06 ± 0.08	0.00	1.29 ± 0.39	2.15 ± 0.29	0.97 ± 0.08	0.33 ± 0.09	0.97 ± 0.30	1.71 ± 0.14	2.68 ± 0.43
ALOHA	Bik <sup>a</sup>	All	0.5 ± 1.1	0.00	0.00	0.00	0.00	0.00	0.00	0.00	0.00	3.1 ± 2.6	0.00	0.00	0.00	0.5 ± 0.8	0.5 ± 0.8
HOT avg <sup>b</sup>	MultiPITS	150	n/a	n/a	n/a	n/a	n/a	n/a	n/a	n/a	n/a	n/a	n/a	n/a	n/a	n/a	
HOT Jun '04 <sup>b</sup>	MultiPITS	150	n/a	n/a	n/a	n/a	n/a	n/a	n/a	n/a	n/a	n/a	n/a	n/a	n/a	n/a	
HOT Aug '04 <sup>b</sup>	MultiPITS	150	n/a	n/a	n/a	n/a	n/a	n/a	n/a	n/a	n/a	n/a	n/a	n/a	n/a	n/a	

(d)															
Site/deployment	Device	Depth	Mass (mg m <sup>-2</sup> d <sup>-1</sup> )	TC (mmole m <sup>-2</sup> d <sup>-1</sup> )	N (mmole m <sup>-2</sup> d <sup>-1</sup> )	P (μmole m <sup>-2</sup> d <sup>-1</sup> )	PI/C (mmole m <sup>-2</sup> d <sup>-1</sup> )	POC (mmole m <sup>-2</sup> d <sup>-1</sup> )	bSi (mmole m <sup>-2</sup> d <sup>-1</sup> )	<sup>234</sup> Th (dpm m <sup>-2</sup> d <sup>-1</sup> )					
K2, 1st	NBST 13	150	963 ± 146	5.4 ± 1.2	0.59 ± 0.13	n/a	0.53 ± n/a	4.88 ± n/a	11.4 ± n/a	1435 ± 135					
K2, 1st	NBST 15	150	896 ± 53	5.4 ± 0.5	0.59 ± 0.05	27.2 ± 4.0	0.47 ± n/a	4.89 ± n/a	10.4 ± n/a	1373 ± 162					
K2, 1st	NBST 17	150	959 ± 123	6.1 ± 0.7	0.72 ± 0.08	34.3 ± 6.9	0.45 ± n/a	5.68 ± n/a	11.1 ± n/a	1217 ± 96					
K2, 1st	NBST 14	300	1102 ± 79	4.6 ± 0.4	0.52 ± 0.05	22.7 ± 10.4	0.48 ± n/a	4.11 ± n/a	13.8 ± n/a	1733 ± 68					
K2, 1st	NBST 16	300	924 ± 120	4.1 ± 0.3	0.47 ± 0.03	24.1 ± 4.5	0.42 ± n/a	3.67 ± n/a	11.5 ± n/a	1650 ± 107					
K2, 1st	NBST 11	500	n/a	n/a	n/a	n/a	n/a	n/a	n/a	n/a	n/a	n/a	n/a	n/a	n/a
K2, 1st	NBST 12	500	490 ± 144	2.6 ± 0.3	0.31 ± 0.01	14.8 ± 5.5	0.20 ± n/a	2.39 ± n/a	5.9 ± n/a	1472 ± 293					
K2, 1st	Clap Trap	150	525 ± 170	4.1 ± 0.3	0.45 ± 0.02	16.5 ± 5.8	0.44 ± n/a	3.64 ± n/a	5.5 ± n/a	1059 ± 78					
K2, 1st	Clap Trap	300	402 ± 113	2.5 ± 0.4	0.29 ± 0.07	11.2 ± 4.7	0.23 ± n/a	2.27 ± n/a	4.6 ± n/a	1069 ± 147					
K2, 1st	Clap Trap	500	421 ± 109	2.9 ± n/a	0.33 ± 0.00	15.3 ± 4.7	0.22 ± n/a	2.69 ± n/a	4.7 ± n/a	1185 ± 100					
K2, 2nd	NBST 13	150	227 ± 53	2.1 ± 1.0	0.27 ± 0.15	21.4 ± n/a	0.04 ± n/a	2.06 ± n/a	2.4 ± n/a	450 ± 81					
K2, 2nd	NBST 15	150	290 ± 20	2.0 ± 0.3	0.23 ± 0.07	16.0 ± 2.7	0.08 ± n/a	1.91 ± n/a	3.4 ± n/a	503 ± 67					
K2, 2nd	NBST 17	150	260 ± 34	1.9 ± 0.1	0.23 ± 0.00	21.8 ± 2.3	0.04 ± n/a	1.81 ± n/a	3.0 ± n/a	487 ± 94					
K2, 2nd	NBST 14	300	222 ± 23	1.3 ± 0.1	0.14 ± 0.02	10.3 ± 0.7	0.04 ± n/a	1.21 ± n/a	2.7 ± n/a	518 ± 118					
K2, 2nd	NBST 16	300	223 ± 69	1.6 ± 0.3	0.17 ± 0.03	13.0 ± 1.0	0.05 ± n/a	1.51 ± n/a	2.6 ± n/a	499 ± 16					
K2, 2nd	NBST 11	500	167 ± 26	1.1 ± 0.1	0.12 ± 0.02	6.1 ± 2.5	0.06 ± n/a	1.01 ± n/a	1.9 ± n/a	591 ± 57					
K2, 2nd	NBST 12	500	219 ± 32	1.2 ± 0.3	0.12 ± 0.01	5.6 ± 1.4	0.05 ± n/a	1.12 ± n/a	2.7 ± n/a	601 ± 11					
K2, 2nd	Clap Trap	150	285 ± 54	2.0 ± n/a	0.27 ± n/a	16.9 ± 0.1	0.05 ± n/a	1.92 ± n/a	3.3 ± n/a	479 ± 40					
K2, 2nd	Clap Trap	300	296 ± 22	1.9 ± n/a	0.24 ± n/a	20.3 ± 3.9	0.08 ± n/a	1.82 ± n/a	3.5 ± n/a	653 ± 88					
K2, 2nd	Clap Trap	500	204 ± 80	1.2 ± n/a	0.13 ± n/a	11.0 ± 0.4	0.07 ± n/a	1.12 ± n/a	2.4 ± n/a	725 ± 133					
K2	Bik <sup>a</sup>	All	28 ± 14	0.34 ± 0.04	0.025 ± 0.004	0.05 ± 0.03	<0.02	~0.34 ± 0.04	4 ± 2	0 ± 17					
K2/HILATS <sup>c</sup>	McLane	150	435 ± 274	n/a	0.19 ± 0.08	n/a	0.018 ± 0.009	1.59 ± 0.57	3.8 ± 2.8	n/a					

(e)														
Site/deployment	Device	Depth	Ba (μg m <sup>-2</sup> d <sup>-1</sup> )	Al (μg m <sup>-2</sup> d <sup>-1</sup> )	Ca (μg m <sup>-2&lt;/sup</sup>									

Table 3. (continued)

K2, 1st	NBST 13	150	n/a	n/a	n/a	n/a	n/a	n/a	n/a	n/a	n/a	n/a	n/a	n/a			
K2, 1st	NBST 15	150	42 ± 17	267 ± 77	28299 ± 5311	182 ± 28											
K2, 1st	NBST 17	150	31 ± 8	188 ± 55	24805 ± 6295	187 ± 67											
K2, 1st	NBST 14	300	78 ± 30	490 ± 180	22336 ± 9448	339 ± 90											
K2, 1st	NBST 16	300	102 ± 5	555 ± 44	28157 ± 5863	250 ± 8											
K2, 1st	NBST 11	500	n/a	n/a	n/a	n/a	n/a	n/a	n/a	n/a	n/a	n/a	n/a	n/a			
K2, 1st	NBST 12	500	124 ± 65	612 ± 318	17460 ± 11555	138 ± 83											
K2, 1st	Clap Trap	150	41 ± 21	378 ± 136	18356 ± 8773	138 ± 93											
K2, 1st	Clap Trap	300	70 ± 36	817 ± 809	12220 ± 3119	209 ± 133											
K2, 1st	Clap Trap	500	132 ± 30	595 ± 155	15045 ± 4405	106 ± 35											
K2, 2nd	NBST 13	150	46 ± n/a	271 ± n/a	4719 ± n/a	60 ± n/a											
K2, 2nd	NBST 15	150	57 ± 2	228 ± 32	4751 ± 12	62 ± 21											
K2, 2nd	NBST 17	150	68 ± 9	207 ± 96	5826 ± 374	74 ± 1											
K2, 2nd	NBST 14	300	87 ± 17	472 ± 17	5626 ± 790	58 ± 14											
K2, 2nd	NBST 16	300	99 ± 10	544 ± 30	8276 ± 983	94 ± 6											
K2, 2nd	NBST 11	500	109 ± 21	516 ± 94	4971 ± 452	94 ± 26											
K2, 2nd	NBST 12	500	92 ± 21	446 ± 154	5146 ± 1219	45 ± 8											
K2, 2nd	Clap Trap	150	55 ± 4	308 ± 145	5704 ± 2210	101 ± 11											
K2, 2nd	Clap Trap	300	140 ± 13	772 ± 38	8845 ± 1191	190 ± 50											
K2, 2nd	Clap Trap	500	203 ± 25	883 ± 115	10996 ± 4684	94 ± 27											
K2	Blk <sup>a</sup>	All	3 ± 2	0 ± 46	558 ± 516	9 ± 8											
K2/HILATS <sup>c</sup>	McLane	150	10.0 ± 9.1	1118 ± 948	28.2 ± 15.8	n/a											
(f)																	
Site/deployment	Device	Depth (m)	CHL c	Per	But	Fuco	Hex	Viola	DDX	Lut	Zeax	MV-Chl b	$\alpha$ -CAR	$\beta$ -CAR	DV-Chl a	MV-Chl a	Tot. Chl a
K2, 1st	NBST 13	150	6.3	0.0	0.5	7.5	3.3	0.0	0.9	0.2	0.7	0.5	0.3	0.6	0.0	19.9	19.9
K2, 1st	NBST 15	150	6.9	0.0	0.7	7.6	3.4	0.0	1.0	0.1	0.6	0.6	0.3	0.6	0.0	25.2	25.2
K2, 1st	NBST 17	150	7.7	0.0	0.6	11.8	3.0	0.0	1.6	0.1	0.7	0.4	0.3	0.8	0.0	26.0	26.0
K2, 1st	NBST 14	300	4.5	0.0	0.6	5.0	3.3	0.0	0.7	0.1	0.5	0.4	0.2	0.4	0.0	12.8	12.8
K2, 1st	NBST 16	300	2.5	0.0	0.3	3.3	2.3	0.0	0.4	0.1	0.5	0.2	0.2	0.3	0.0	7.9	7.9
K2, 1st	NBST 11	500	n/a	n/a	n/a	n/a	n/a	n/a	n/a	n/a	n/a	n/a	n/a	n/a	n/a	n/a	n/a
K2, 1st	NBST 12	500	1.5	0.0	0.3	3.5	1.9	0.0	0.4	0.1	0.4	0.3	0.1	0.4	0.0	6.6	6.6
K2, 1st	Clap Trap	150	3.5	0.0	0.5	4.6	3.1	0.0	0.5	0.1	0.3	0.6	0.2	0.4	0.0	11.8	11.8
K2, 1st	Clap Trap	300	1.7	0.0	0.3	3.1	1.9	0.0	0.4	0.0	0.3	0.4	0.1	0.3	0.0	6.7	6.7
K2, 1st	Clap Trap	500	2.5	0.0	0.2	2.3	1.7	0.0	0.3	0.1	0.3	0.3	0.2	0.3	0.0	8.4	8.4
K2, 2nd	NBST 13	150	1.0	0.0	0.2	1.5	1.3	0.0	0.2	0.0	0.2	0.2	0.1	0.1	0.0	5.1	5.1
K2, 2nd	NBST 15	150	1.9	0.0	0.3	1.8	1.9	0.0	0.3	0.0	0.2	0.3	0.2	0.2	0.0	8.2	8.2
K2, 2nd	NBST 17	150	1.4	0.0	0.3	2.6	1.9	0.0	0.2	0.0	0.2	0.4	0.1	0.1	0.0	7.6	7.6
K2, 2nd	NBST 14	300	0.8	0.0	0.1	1.0	1.0	0.0	0.1	0.0	0.1	0.1	0.1	0.1	0.0	3.6	3.6
K2, 2nd	NBST 16	300	1.0	0.0	0.2	1.2	1.3	0.0	0.2	0.0	0.1	0.2	0.1	0.1	0.0	4.2	4.2
K2, 2nd	NBST 11	500	0.6	0.0	0.1	0.9	0.8	0.0	0.1	0.0	0.1	0.1	0.1	0.1	0.0	2.8	2.8
K2, 2nd	NBST 12	500	n/a	n/a	n/a	n/a	n/a	n/a	n/a	n/a	n/a	n/a	n/a	n/a	n/a	n/a	n/a
K2, 2nd	Clap Trap	150	1.6	0.0	0.5	1.9	2.2	0.0	0.3	0.0	0.2	0.5	0.1	0.2	0.0	7.4	7.4
K2, 2nd	Clap Trap	300	1.6	0.0	0.3	1.2	1.8	0.0	0.3	0.0	0.1	0.5	0.1	0.3	0.0	6.0	6.0
K2, 2nd	Clap Trap	500	0.8	0.0	0.2	0.6	0.9	0.0	0.1	0.0	0.1	0.2	0.1	0.1	0.0	5.2	5.2
K2	Blk <sup>a</sup>	All	n/a	n/a	n/a	n/a	n/a	n/a	n/a	n/a	n/a	n/a	n/a	n/a	n/a	n/a	n/a
K2/HILATS <sup>c</sup>	McLane	150	n/a	n/a	n/a	n/a	n/a	n/a	n/a	n/a	n/a	n/a	n/a	n/a	n/a	n/a	n/a

Pigment abbreviations, Chl c: chlorophyll c; Per: peridinin; But: 19'-butanoyloxyfucoxanthin; Fuco: fucoxanthin; Hex: 19'-hexanoyloxyfucoxanthin; Viola: violaxanthin; DDX: diadinoxanthin; Lut: lutein; Zeax: zeaxanthin; MV-Chl b: monovinyl chlorophyll b; DV-Chl a and MV-Chl a: di- and monovinyl chlorophyll a, respectively;  $\alpha$  and  $\beta$ -Car: alpha and beta carotene, respectively.

<sup>a</sup> The blank ("Blk") values are taken from the covered, process blank tubes on board the Clap Traps. The magnitude of the blank is divided by the nominal deployment time (3, 4, 5 days for 150, 300 and 500 m, respectively) to get a blank "flux" to compare to the measured sample fluxes.

<sup>b</sup> Hawaii Ocean Time Series (HOT) data taken from website: <<http://hahana.soest.hawaii.edu/hot/hot-dogs/interface.html>>. Used without correction.

<sup>c</sup> Data from Honda et al., 2006. The values shown in the table are from the HILATS-K2 sampling period of July 24–August 20, 2005. Values displayed are corrected for 20% collection efficiency, as suggested in Honda et al., 2006.

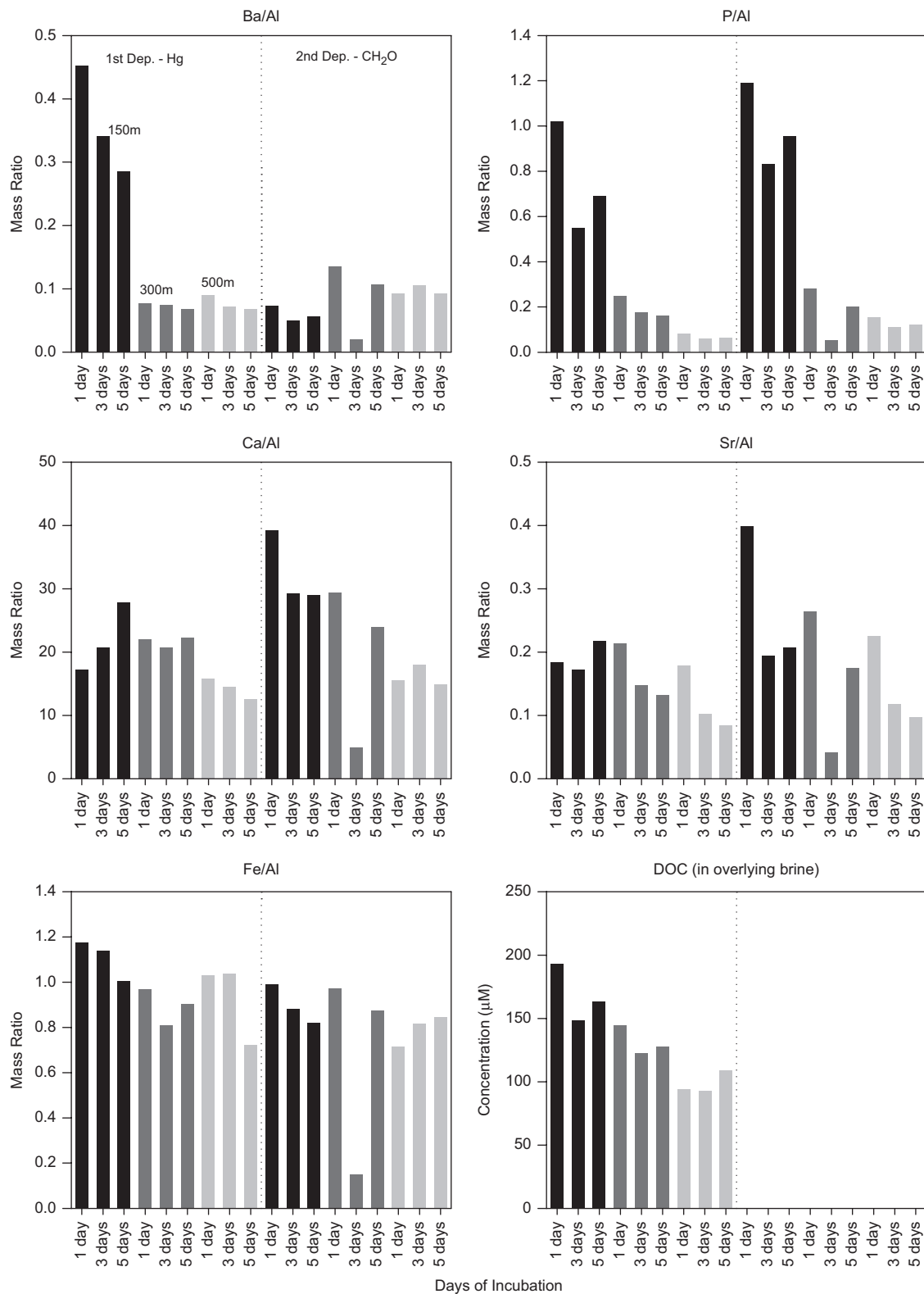


**Fig. 3.** Results from poisoned trap material aging experiments from ALOHA. Trap material was wet split as with the other samples, but then held as a water/particle mixture for a number of days before being processed. The graph illustrates the relative loss of material from the filterable phase as might occur during the deployments. Results from K2 (not shown) suggested little attenuation over time.

results, Buesseler et al. (2007a) suggest that, when possible, shorter deployment times and rapid processing are important, such as used during VERTIGO, in reducing the chance for continued particle break up and solubilization even in poisoned/preserved samples.

#### 4.1.2. "Swimmer" biomass in-trap material

An enduring problem in collecting sinking particles is the incidental "collection" of a variety of zooplankton that actively enter the trap (e.g., Karl and Knauer, 1989). The poison/preservatives that are added are effective at killing the variety of

zooplankton that enter the trap and reach the brine layer at the bottom of the tube. These "swimmers" then become part of the material collected from the tube and should not be included in estimates of the passive downward flux of various components. For this reason, and as noted in Section 3.2, the trap material was passed through a 350 μm screen to remove most of these animals. However, some of the swimmers were small enough to pass through this screen. To assess the magnitude of the small swimmer artifact, one of the sample splits ("d"; Table 2) was examined under a microscope and any remaining swimmers were removed manually. The material caught on the 350 μm screen was

**Table 4**

Apparent flux correction percentages as suggested by poisoned trap material aging experiments on ALOHA particles

Element	Deployment	Depth (m)	Apparent correction (%)
Ba	1	500	23±7
Ba	2	150	14±6
P	2	300	20±3
P	2	500	16±7
Mn	1	500	47±14
Fe	1	500	24±7
Sr	2	150	33±11
Sr	2	300	17±5
Sr	2	500	48±13

Elements/deployments not shown in the table required less than 10% correction (including all samples from K2). These values shown for illustration, with no actual corrections made to values in Table 3.

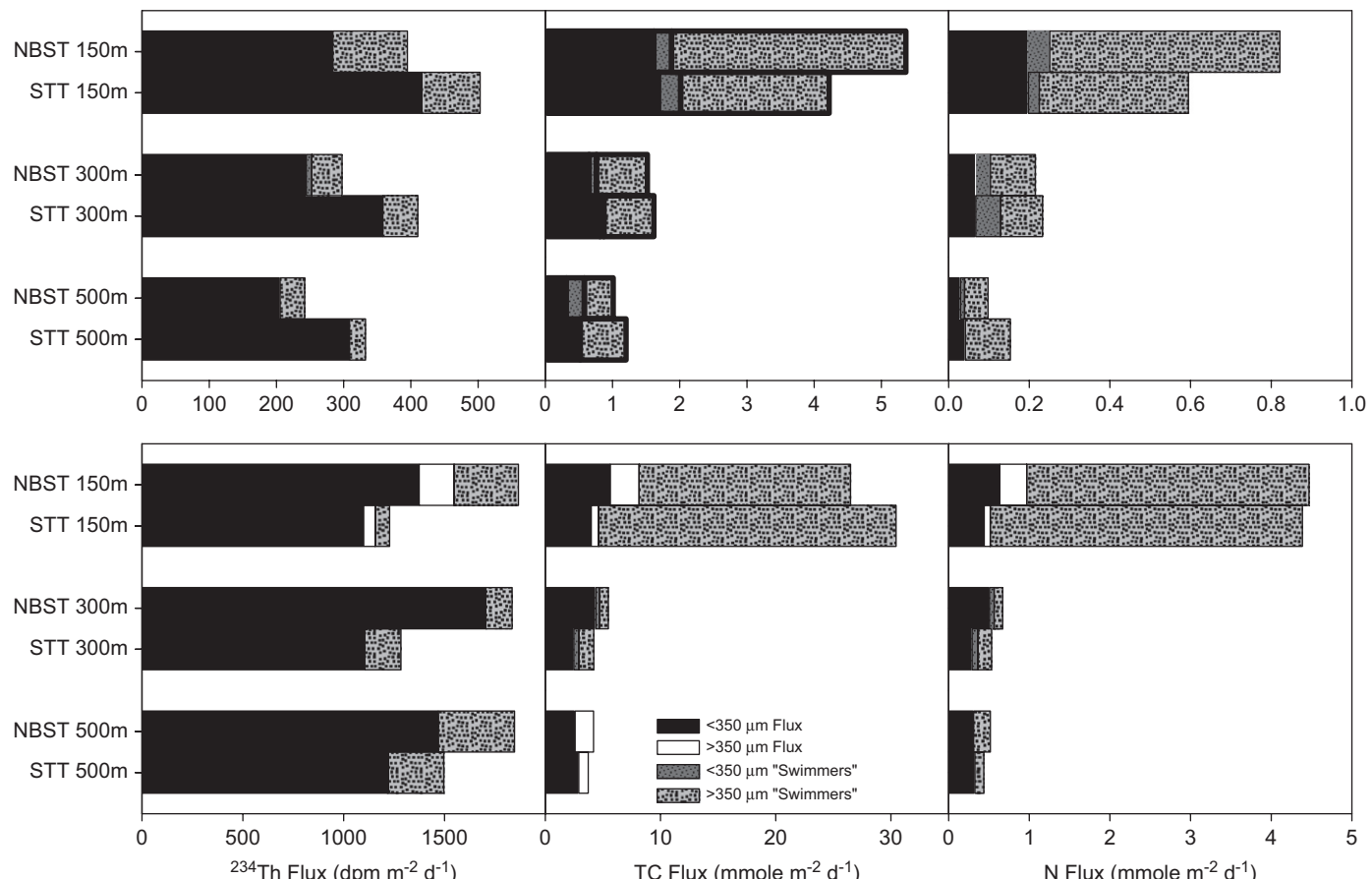


**Fig. 4.** The  $^{234}\text{Th}$ , total carbon (TC) and N associated with various fractions of material collected in VERTIGO sediment traps. The collected material was first passed through a 350 μm mesh screen to remove large zooplankton "swimmers." However, some non-zooplankton material, which was likely passively sinking material and legitimate flux, was observed to have stuck to these screens as well (the " $>350\text{ }\mu\text{m}$  flux"). Of the material that passed through the screen, a small amount was actually zooplankton that likely swam into the sediment traps (determined by whole, well preserved carcasses), and that should not be included in the flux estimates (" $<350\text{ }\mu\text{m}$  swimmers").

also examined and zooplankton swimmers were separated from the sinking material in order to determine if significant detrital material was caught by these screens. These various fractions were then processed for C, N and  $^{234}\text{Th}$  (Fig. 4).

With these processing steps, we can thus compare in the same units, the actual detrital flux, to the quantity of C, N and  $^{234}\text{Th}$  removed on the screen, i.e. large swimmers ( $>350\text{ }\mu\text{m}$ ) vs. small swimmers ( $<350\text{ }\mu\text{m}$ ), and detrital material caught on the  $>350\text{ }\mu\text{m}$  screen. A number of interesting trends were observed. First, the  $>350\text{ }\mu\text{m}$  swimmer "flux" was often very large relative to the passive sinking material (up to 8.75 times more), especially for C and N, and illustrates the importance of a swimmer removal step in accurately determining the true sinking flux. This finding is not unexpected, but most trapping protocols do not quantify the amount of swimmers removed. Over a range of flux environments, Buesseler et al. (2007a) summarized prior studies and found 14–90% of the total POC caught in traps can be attributed to swimmers.

At both sites, the amount of this swimmer material was greater at 150 m than at the deeper depths, which is consistent with decreasing swimmer biomass collected by MOCNESS plankton tows during the cruises (Steinberg et al., this volume). It is interesting to note that the amount of swimmer biomass collected in the sediment traps appears to attenuate more quickly with depth at K2 than at ALOHA, in contrast to the MOCNESS profiles. Examination of the animals collected below 150 m at K2 indicated that many were in diapause or dead (Kobari et al., this volume), and therefore not attracted to feed in the traps. This could suggest,

however, that some of the swimmer biomass at K2 could have been considered part of the true sinking flux for that site. The amount of C, N and  $^{234}\text{Th}$  contributed by small swimmers ( $<350\text{ }\mu\text{m}$ ) was generally insignificant relative to the passively sinking ("true") flux material, with the exception of N in the 300 m Clap Trap from ALOHA (ca. 50%). We have therefore made no attempt to correct the values reported in Table 3 for what would represent a small positive bias due to artifacts related to small swimmers. We saw little evidence for passively sinking material that had been accidentally caught on our 350  $\mu\text{m}$  screen at ALOHA, and only a small amount of this " $>350\text{ }\mu\text{m}$  flux" at K2 that would be a negative bias on the detrital flux results.

These experiments indicate that our wet screening procedures were effective at separating zooplankton from passive particles in our samples with only small positive and negative biases. In other settings there may be a larger flux of small swimmers, or higher fraction of "true" flux material caught on the screen, so this should be confirmed in any study. In the only such comparison we have found, the POC flux at BATS in "picked" traps (i.e. manual removal under a microscope) was 40% lower than when 350  $\mu\text{m}$  screening alone was used (20% lower for PON), suggesting more small swimmers at this particular site (Buesseler et al., 2007a).

As seen in earlier studies (e.g., Buesseler et al., 1994), most of the  $^{234}\text{Th}$  collected in the traps was associated with passive sinking material and not swimmers. This is consistent with studies that show Th binding preferentially to polysaccharide functional groups, which are abundant in marine snow, rather than all surfaces (Santschi et al., 2006), and experiments that indicate Th is not assimilated by zooplankton very effectively during feeding (e.g., Wang et al., 1996).

#### 4.1.3. Poison/preservative differences

Table 3 provides a summary of all flux results. No systematic difference was seen in the apparent flux of mass or elemental composition between the two poison/preservative treatments on board of any individual device, as illustrated in Fig. 5 with mass fluxes from both sites and including all devices. Thus, Table 3 shows data on the average flux of both types of poisoned tubes (when available), and therefore represents the values of 1–4 individual tubes. As can be seen in the table, however, there were device-to-device differences that were significant.

#### 4.1.4. Differences between devices

One feature common to the flux measurements at both sites was variability, both between tubes on a single device and between devices. As noted above, there are certainly differences between the free and tethered devices at some depths/times, but there is variability even within the NBST data alone. This is illustrated in Table 5, which displays the variability between splits, tubes and devices using mass and  $^{234}\text{Th}$ , the two parameters measured in replication at all these scales. The variability is similar at all of these measured scales, suggesting that inherent variability is likely limiting our ability to refine the flux estimates of these two parameters (and by extension, all others as well). By employing at-sea pooling/wet splitting, we have improved the precision of measurements from any one device above that of other trapping programs. Other methodological improvements could be made. For example, as swimmer material is often a large percentage of the total amount of mass in the trap, small inefficiencies in screening could contribute significant sample-to-sample differences in the screen-passing fraction. Ultimately, however, inherent variability appears to pose a considerable challenge to accurately characterizing the average absolute magnitude of property fluxes with a precision better than 10–20%. It would appear that the principal way of tackling

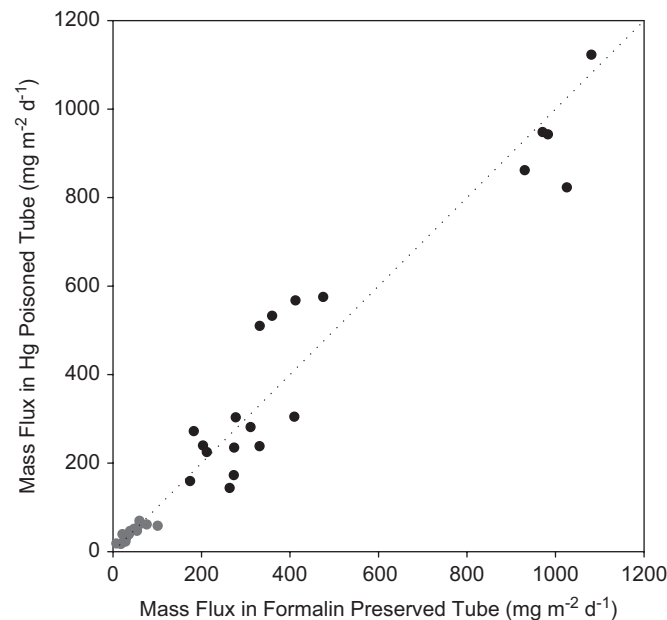


**Fig. 5.** The correlation of mass flux measurements made in tubes from the same sediment trap device but poisoned/preserved with either  $\text{HgCl}_2$  or formalin. Correlations were in general good for other parameters measured as well, and results from the two kinds of tubes were combined to form device averages included in Table 3.

**Table 5**  
Examination of the scales of variability in sediment trap data

Comparison	Mass (%)	$^{234}\text{Th}$ (%)
Split-to-split	$13 \pm 20$	$12 \pm 14$
Tube-to-tube	$17 \pm 13$	$13 \pm 10$
Device-to-device	$17 \pm 17$	$11 \pm 8$

NBST data only.

this issue is to increase the extent of replicate sampling, as we have done in VERTIGO. This approach has also recently been suggested to be the best way to refine modeling of flux attenuation and removing a functional form bias that is inherent to the problem of describing mesopelagic cycling (Primeau, 2006).

Differences are evident at times when correlations are calculated between average NBST and average Clap Trap fluxes for a range of trap components (Table 6). At ALOHA, while correlation coefficients were not always high, none of the regression slopes were significantly different from 1 at  $\alpha = 0.05$ . The situation at K2 was much different, however, with all components except PIC showing significantly lower fluxes measured in the tethered traps during the 1st deployment at 150 and 300 m, but mostly good agreement in the 2nd deployment (except P, and Al and Th which had higher fluxes in the Clap Traps than the NBSTs). The biomass and primary production in the surface waters (Boyd et al., this volume; Elskens et al., this volume) as well as the flux in the NBSTs were observed to drop from the 1st to 2nd deployments, while the flux in the Clap Traps did not change significantly. The deep moored traps at this site also showed the same sharp decrease in flux during this time (Honda, pers. comm.). This suggests strongly that the trapping efficiency of the tethered traps was poorer than the NBSTs in the 1st deployment, giving rise to lower correlation slopes. As will be discussed in greater detail below, the composition of the material did not significantly change between deployments for the two

**Table 6**

Site	Variable	RMA slope
ALOHA	Mass	0.90±0.10
	POC	0.91±0.09
	PIC	1.39±0.27
	bSi	0.98±0.24
	N	0.94±0.12
	P	0.77±0.14
	Al	0.88±0.23
	$^{234}\text{Th}$	0.92±0.20
K2, 1st	Mass	0.31±0.13
	POC	0.56±0.19
	PIC	1.04±0.35
	bSi	0.17±0.07
	N	0.58±0.19
	P	0.37±0.16
	Al	0.46±0.15
	$^{234}\text{Th}$	0.30±0.13
K2, 2nd	Mass	1.04±0.29
	POC	0.67±0.20
	PIC	0.84±0.30
	bSi	1.04±0.34
	N	1.06±0.22
	P	0.53±0.17
	Al	1.91±0.25
	$^{234}\text{Th}$	2.10±0.54

Values greater than 1 indicate greater fluxes for Clap Traps, while lower than 1 indicate greater fluxes for NBSTs.

major phases at either site, even though at K2 the absolute fluxes in the NBSTs did change. It would appear, therefore, that the lower Clap Trap collection efficiencies at K2 at 150 and 300 m for deployment 1, resulted in quantitative but little qualitative difference between devices.

**Table 7** illustrates the average, standard deviation, maximum and minimum in speeds and tilts of the FSI current meters deployed below the Clap Traps collecting 2 samples min<sup>-1</sup>. It should be noted that the current meters and the tube arrays were not fixed together but separated by chain below the arrays, and therefore the tilts should be interpreted as upper limits. In general, higher slip speeds and tilts were observed at ALOHA than at K2, and little difference was seen between deployments at K2. Thus, the current meter data do not support the hypothesis that trapping systems experiencing higher hydrodynamic slip will exhibit poor collection efficiencies, and thus the cause of the lower Clap Trap fluxes during deployment 1 at K2 remain unresolved.

In summary, in three out of four deployments of untethered and tethered traps, the NBST and Clap Trap fluxes agreed fairly well. These three deployments were characterized by fluxes of similar magnitude. The one deployment where the systems did not agree, was also the period of highest fluxes at K2 (deployment 1). Some of us have previously noted that tethered traps can both over- and under-collect sinking particles (Buesseler, 1991; Buesseler et al., 2000) and underlying causes of this collection bias are likely quite complex. A recent compilation of  $^{234}\text{Th}$  derived trapping efficiencies (Buesseler et al., 2007a) suggests that while both over- and under-collection are observed, the mean difference is a factor of two under-collection for tethered traps, which is in the same direction and magnitude as we see during D1 at K2. Our discussions will focus mostly on the NBST data in this manuscript, though the Clap Trap results are shown as well since they agree to a large extent. Thus, the comparison of two sampling platforms in VERTIGO offers no clear conclusion regarding when and why

**Table 7**

Speed and tilt of the tethered sediment trap arrays through the water as measured by an FSI current meter deployed below the array

Site/depth/deployment	Average Clap Trap speed [max/min] (cm s <sup>-1</sup> )	Average Clap Trap tilt [max/min] (degrees from vertical)
ALOHA/150 m/1st	n/a	n/a
ALOHA/300 m/1st	6.3±3.2 [14.8/0.1]	4.0±2.4 [13.4/0.1]
ALOHA/500 m/1st	26.4±6.8 [51.2/13.8]	4.0±2.6 [13.5/0.9]
ALOHA/150 m/2nd	5.7±2.8 [15.6/0.1]	6.1±4.6 [27.5/0.4]
ALOHA/300 m/2nd	n/a	n/a
ALOHA/500 m/2nd	7.0±2.9 [16.7/0.1]	11.4±6.8 [34.9/1.0]
K2/150 m/1st	3.3±1.5 [8.2/0.01]	2.6±1.3 [6.9/0.1]
K2/300 m/1st	4.3±1.9 [11.5/0.1]	3.9±2.2 [13.2/0.2]
K2/500 m/1st	5.0±1.9 [10.4/0.6]	2.5±1.7 [9.8/0.4]
K2/150 m/2nd	4.6±1.9 [9.5/0.2]	5.4±3.7 [17.0/0.2]
K2/300 m/2nd	5.4±1.9 [10.5/0.1]	6.7±2.6 [16.4/3.0]
K2/500 m/2nd	4.4±2.1 [12.2/0.1]	2.8±2.7 [14.8/0.1]

tethered systems might not exhibit 100% collection efficiency, but suggest that high flux conditions rather physical forcing were responsible for Clap under-collection. More comparisons of free and tethered systems appear to be necessary to help resolve this long-standing issue.

#### 4.2. Flux results

The vertical profiles of flux for both sites are shown in [Figs. 6 and 7](#). In all these figures, a common plotting convention is used: NBST values are represented by circles and Clap Trap by triangles, and the 1st deployments are displayed as being at a shallower depth for clarity. Error bars represent the standard deviation of 2 determinations (4 in the case of mass) of each parameter when available. Some of this data has appeared already, but only in summary form (Buesseler et al., 2007b).

##### 4.2.1. Flux variability within each site

The trap fluxes at ALOHA were similar between the deployments, a result which was consistent with our observations of relatively constant chlorophyll concentrations, primary and new production and zooplankton biomass (Boyd et al.; Buesseler et al.; Elskens et al.; Steinberg et al.; all in this volume). The reported fluxes from the HOT-DOGS database of the Hawaii Ocean Time Series Program (<http://hahana.soest.hawaii.edu/hot/hot-dogs/interface.html>) from 1988 to 2005 for mass, carbon, nitrogen, phosphorus, silica and particulate inorganic carbon at 150 m are included in [Table 3](#) for comparison to the VERTIGO data. As part of HOT during the summer of 2004, successful PITs deployments were made in mid-June and mid-August, and these values are also included in [Table 3](#). The VERTIGO measurements at 150 m compare well with these average and contemporaneous HOT data.

Unlike ALOHA, the fluxes at K2 were very different between the two deployments, with the first being much higher for most particle components. For example, fluxes of mass, POC, N, P, PIC (and Ca), bSi, Sr all dropped by factors of 2–5 in NBSTs. The fluxes of Al (and other metals), however, remained nearly constant between deployments (Lamborg et al., this volume).

A moored McLane, multi-sample, time-series style conical sediment trap (and bio-optical) array was also in operation at K2 during our occupation, as part of the JAMSTEC time-series program at K2 (Honda et al., 2006; Honda et al., personal comm.). Honda and colleagues observed mass and component fluxes that are significantly (ca. 5 ×) lower than our measured fluxes for the same time period and depth, but they also estimated their

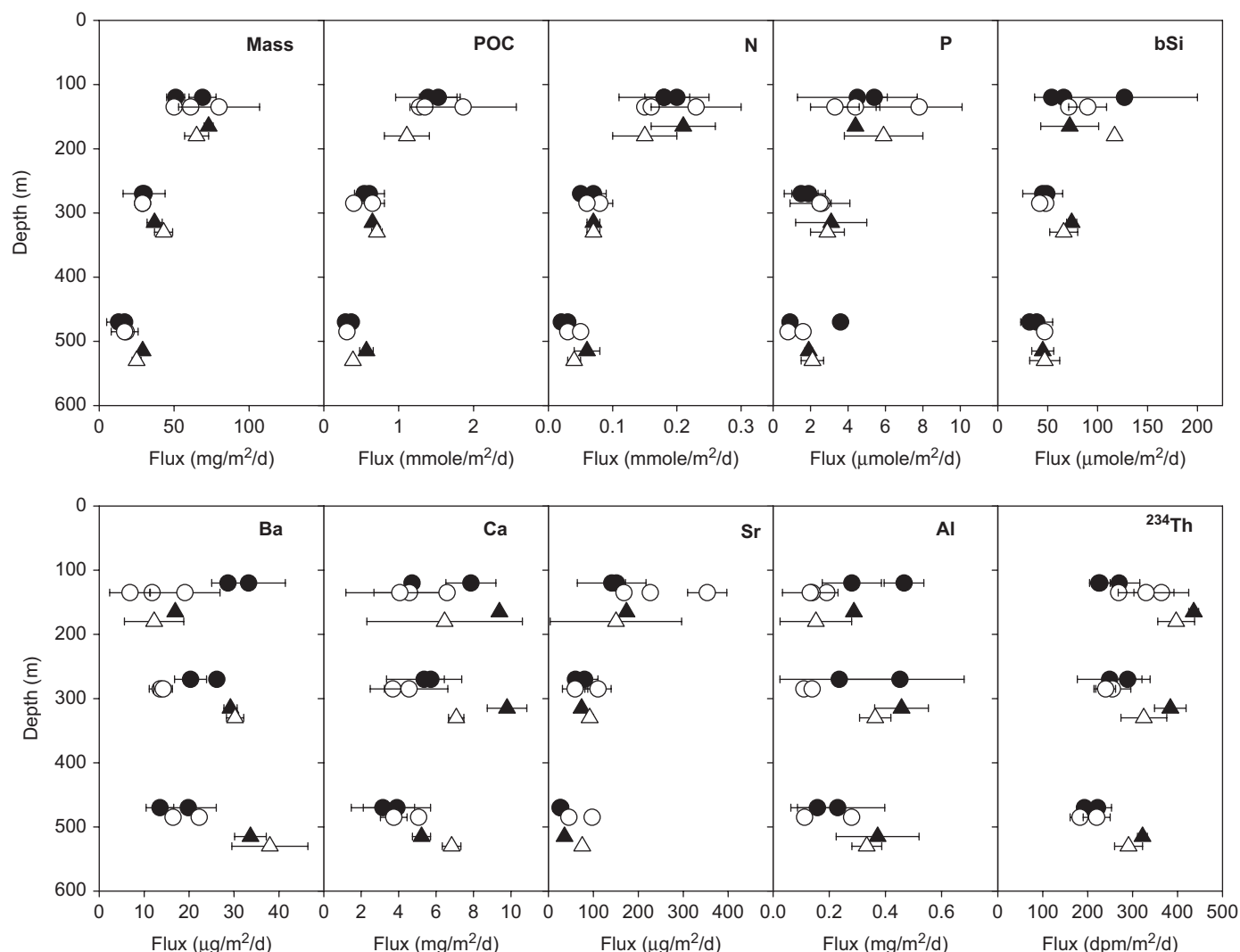


**Fig. 6.** Measured fluxes at ALOHA. The plotting convention for this figure and Fig. 7 include placing the NBSTs (circles) at shallower depths than the Clap Traps (triangles), and with the first deployments shallower than the second. All traps were deployed to nominally the same depths, however. Error bars are 1 SD.

trapping efficiency to be  $20 \pm 7\%$ , based on the measured  $^{230}\text{Th}$  flux. With correction, then, their flux values agree well with ours. The JAMSTEC deep traps also showed a sharp decline in the flux during the same period as we observed the decrease in biomass, productivity and NBST fluxes (Buesseler et al., this volume). Furthermore, the major component composition of the JAMSTEC samples were also very similar to ours (see description below).

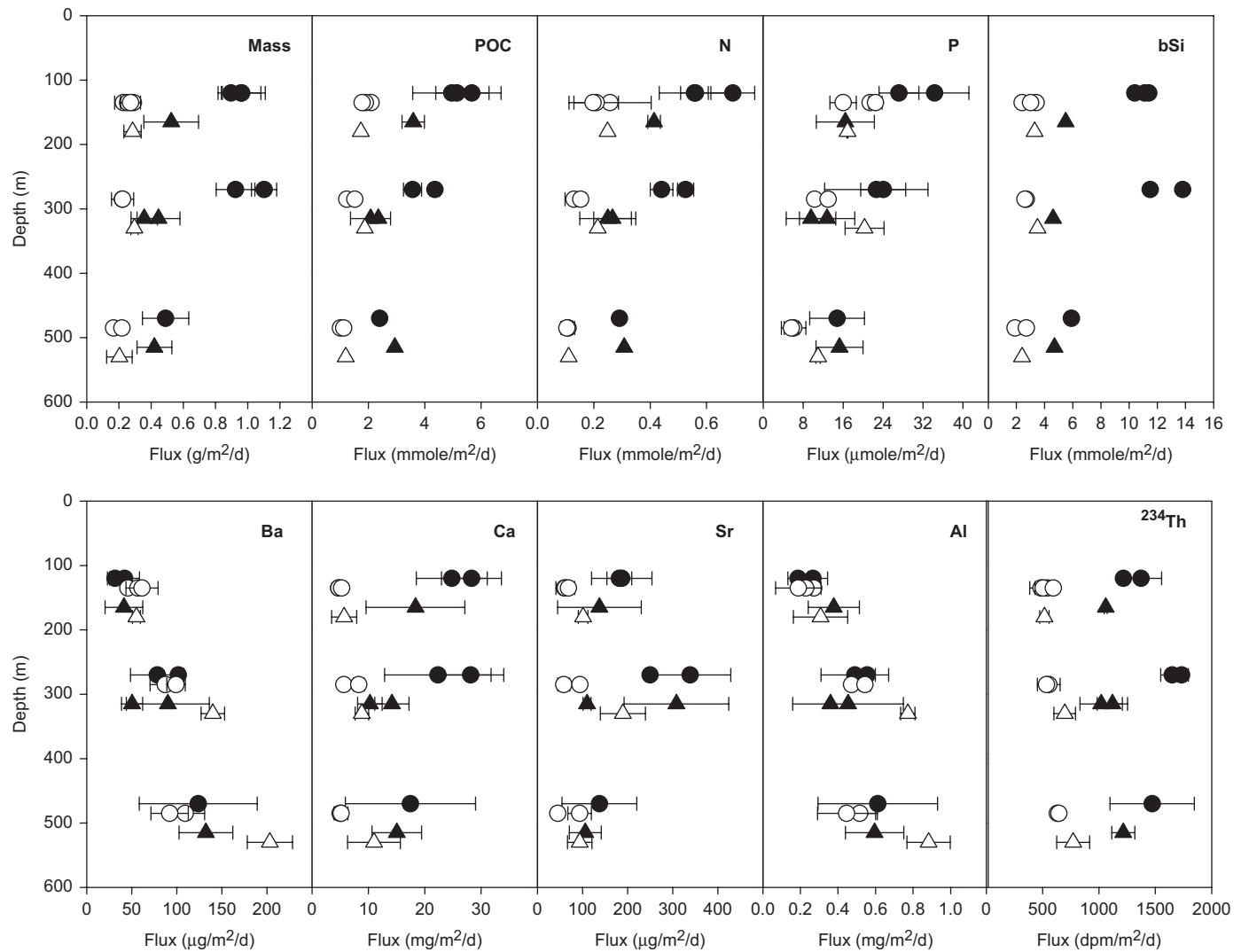
#### 4.2.2. Major phases and mass flux

Fig. 8 illustrates the relative abundances of 4 major flux components by weight that were found in the sediment trap samples at both sites. The measured POC, bSi, PIC and Al were converted to particulate organic matter (POM), opal,  $\text{CaCO}_3$  and lithogenic material by multiplying the mass fluxes by 2.2, 2.4, 8.33 and 12.56, respectively (for POM: Klaas and Archer, 2002; for opal: Mortlock and Froelich, 1989; for lithogenics: Wedepohl, 1995). The sum of these compared well with the measured total mass flux (the height of the stacked bars in Fig. 8 shows the agreement), though at ALOHA, the agreement is more variable, in part due to lower mass fluxes per sample. Two samples at ALOHA (1st deployment Clap Trap at 150 m and 2nd deployment NBST at 500 m) look anomalous in Fig. 8 because no organic/inorganic carbon data are available. The mass of ALOHA material was dominated by organic matter (ca. 40–70%), with decreasing %POM

with depth. The next most important phases with respect to mass were  $\text{CaCO}_3$  (ca. 15–35%), with opal and lithogenic material contributing in approximately equal abundance to the mass flux (ca. 10%). This is in stark contrast to K2, where sinking mass was dominated by opal (ca. 80%), organic matter comprised about 10%, and carbonate and lithogenics less than about 6% to the total mass flux. A large difference between deployments was seen in  $\text{CaCO}_3$  at K2, with its contribution to mass dropping about 3-fold as the absolute total mass flux dropped by 3-fold as well. This difference between ALOHA and K2 is not surprising given the prevalence of diatoms and radiolarian at K2, and smaller, generally non-mineral forming cells at ALOHA (Steinberg et al., this volume; M.W. Silver, pers. comm.).

#### 4.2.3. Flux attenuation characteristics 1: decreasing fluxes with depth

Decreasing flux curves with depth are commonly observed for C, N and P as a result of the disaggregation or degradation of sinking organic matter (e.g., Martin et al., 1987). The flux attenuation curves in VERTIGO however, exhibit 3 different patterns: decreasing flux with depth (macronutrients, Ca and Sr), constant with depth (Al in ALOHA), and increasing with depth (Ba and Al at K2). The two sites differed significantly in the extent of particle flux attenuation within the mesopelagic (Buesseler



**Fig. 7.** Measured fluxes at K2. Plotting convention as in Fig. 6.

et al., 2007b). This is perhaps best illustrated by normalizing the fluxes during each of the deployments to the flux at 150 m, shown for POC in Fig. 9. Much more of the POC flux at ALOHA is lost between 150 and 500 m than at K2 (20% and 21% compared to 46% and 55%). It is also interesting to note that the shapes of the attenuation curves for each site are the same between deployments, even between the high and low flux deployments at K2, suggesting that the controls on flux attenuation were constant between deployments.

The difference in flux attenuation between ALOHA and K2 is not as striking at the base of the euphotic zone, however. The “e-ratios” of the two sites, the ratio of export flux to primary production, were fairly similar, except the 1st deployment at K2 which was higher than the other three deployments (flux 150 m/PProd ~10%; Buesseler et al., 2007b; Boyd et al., this volume). If we account for the fact that the euphotic zone is much shallower at K2 (50 m) than ALOHA (125 m) than the e-ratio defined by export out of the euphotic zone is higher at K2, especially for D1 (up to 21%; Buesseler et al., this issue). As described by their *b* values (see below), the two sites differ a great deal in the relative amount of POC that is able to traverse the mesopelagic zone, with much more of the export flux at K2 making its way to 500 m (Buesseler et al., 2007b). When these two features are combined,

K2 clearly transports more of the carbon fixed in the euphotic zone to below 500 m than does ALOHA.

An additional way of quantitatively comparing the curve shapes between components and sites is to calculate a remineralization length scale or fit the data with a functional form that can be used to approximate this parameter. One of the most commonly cited functions for describing particle flux profiles in the ocean is a power law of the form (Martin et al., 1987):

$$F_z = F_{z0} \left( \frac{z}{z_0} \right)^{-b}$$

where *z* is a reference depth (100 m is often used) and *b* is the power-law exponent and determines the curve shape. The non-linear least squares fits for *b* for both sites and all components are shown in Table 8.

A number of interesting trends in *b* values are evident. First, both sites exhibit the same trend in *b* values for the major component phases: Chl *a*>POC>mass>biogenic Si>PIC>Al (Buesseler et al., 2007b). In this functional form, the larger the *b* value, the more rapid the attenuation with depth (i.e., the shorter the remineralization length scale) and therefore organic matter appears to experience a greater degree of flux attenuation than

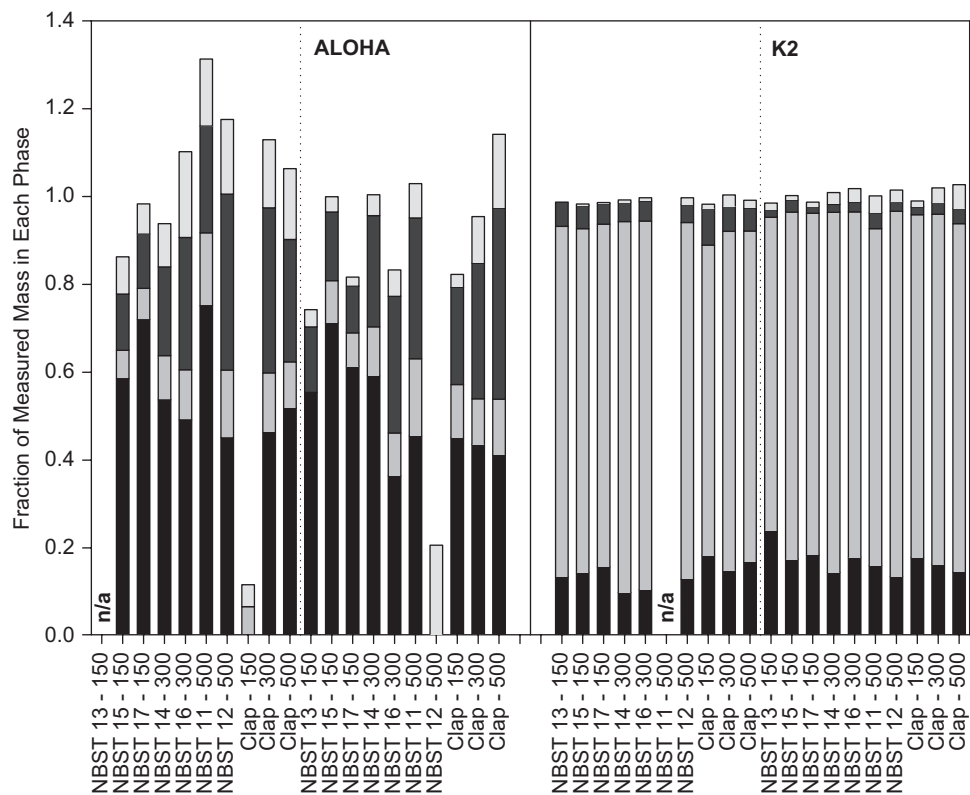


**Fig. 8.** Relative contributions of the major phases of sinking mass at ALOHA (left set) and K2. Bars, in order from the bottom are: black, organic matter; light gray, opal; dark gray, calcium carbonate; white, lithogenic (assumed crustal) material. Values are the fraction of the independently measured mass represented by each phase estimated from the organic carbon (organic matter), biogenic silica (opal), particulate inorganic carbon (calcium carbonate) and Al (lithogenics) measured fluxes.

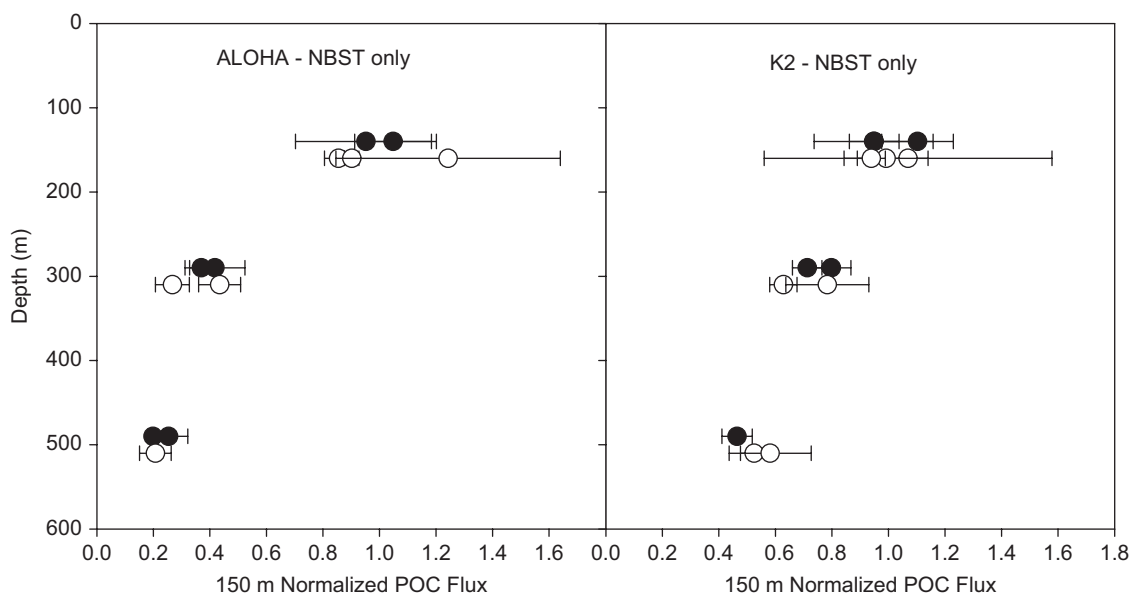


**Fig. 9.** The example of 150 m normalized particulate organic carbon (POC) flux at both sites, illustrating the difference in curve shape through the mesopelagic zone. This difference in flux attenuation is summarized by fitting a power law through the data and reporting the exponent as a metric of apparent remineralization length scale for all components in Table 3. NBST data only are included, with the first deployment at each site shown at a shallower depth and in black symbols.

most other components, with Chl *a* taken to be a representative of the most labile fraction of the sinking organic matter.

Through comparison to deep sediment trapping programs of others (Honda et al., 2006; Buesseler et al., 2007b, this volume; Honda et al., pers. comm., Karl et al., unpublished results), it is also clear that much of the attenuation of biogenic material flux that takes place below the euphotic zone does so within the

mesopelagic zone. At ALOHA, 80% of shallow export was lost within the mesopelagic, with only an additional 20–40% of the flux leaving 500 m being lost by 4000 m. At K2, about half the shallow export was lost in the mesopelagic, with roughly half of that leaving 500 m reaching 4000 m.

The major biomimetic phases, and the elements that track them, opal (Si), celestite (Sr) and calcite/aragonite (PIC and Ca)

**Table 8**

Summary of power-law exponent values for non-linear fits of vertical flux data

Component	ALOHA "b"	K2 "b"
Al	0.51±0.29/-0.08±0.27	-0.92±0.21/-0.66±0.16
Ba	0.52±0.15/-0.40±0.25	-1.09±0.20/-0.51±0.12
bSi	0.65±0.22/0.53±0.19	0.31±0.24/0.20±0.12
Ca	0.44±0.19/0.13±0.15	0.29±0.15/-0.05±0.16
Fuco	2.05±0.10/0.98±0.29	0.86±0.23/0.68±0.19
Mass	1.14±0.13/1.06±0.11	0.36±0.22/0.24±0.09
N	1.68±0.13/1.27±0.18	0.52±0.11/0.59±0.07
P	0.88±0.48/1.17±0.27	0.55±0.13/0.97±0.12
PIC	0.37±0.29/0.24±0.12	0.55±0.21/-0.04±0.21
POC	1.25±0.09/1.36±0.21	0.57±0.10/0.49±0.07
Sr	1.40±0.14/1.11±0.32	0.04±0.38/-0.02±0.22
Tot. Chl <i>a</i>	1.88±0.16/1.10±0.31	1.10±0.18/0.76±0.17
Zeax	1.43±0.13/1.16±0.29	0.42±0.06/0.69±0.14

Only values for NBSTs are included. Values are 1st deployment/2nd deployment ±1 S.E.

were also seen to decrease in flux with depth. For two of these phases, opal and celestite, seawater is everywhere undersaturated. In the case of opal, dissolution rates of diatom biogenic silica have been measured to range from 0.8% to 18% d<sup>-1</sup>, when colonized by bacteria (Bidle and Azam, 1999). These measured dissolution rates are, at the extreme, consistent with the observed opal flux attenuation within the mesopelagic at both sites (roughly 40% lost, implying a mesopelagic residence time of 2–50 days and therefore sinking rates of 7–175 m d<sup>-1</sup>). However, Bidle and Azam's average dissolution rates (ca. 2% d<sup>-1</sup>, 2 days after colonization) appear too slow to explain the opal loss in the mesopelagic at both sites given canonical sinking rates (ca. 100 m d<sup>-1</sup>) and those measured during VERTIGO using an indented rotating sphere sediment trap (>50% of material sinking faster than 140 m d<sup>-1</sup>; Peterson et al., 2005; Trull et al., this volume). This suggests that, in addition to bacterial degradation, disaggregation/grazing is required to explain the disappearance of opal, or degradation rates are faster than prior experiments suggest. Similar studies of celestite dissolution kinetics are lacking, but the large degrees of undersaturation (e.g., Monnin and Cividini, 2006) and rapid attenuation of Sr relative to other components suggest that dissolution may be an adequate explanation for the flux attenuation curve for this biominer. The common occurrence of acantheria (with celestite tests) in shallow waters yet their absence in shallow traps is a common observation in other studies unless Sr is added to the trap solution to inhibit dissolution (Michaels et al., 1995).

The decrease in Ca (and PIC) flux was not large at either site, and appeared less than for bSi. This is somewhat surprising as within the mesopelagic, aragonite is undersaturated at both sites, and calcite as well at K2 (Feely et al., 2002). Only about half the sinking Ca flux can be explained by PIC and dust. The remainder (Ca<sub>xs</sub>) does not correlate with either POC or P, and has ratios that are much higher than suggested in extended "Redfield" ratios for a variety of cell types (ca. 0.1 Ca:P, mole:mole; e.g., Ho et al., 2003; Finkel et al., 2006). ALOHA ratios (ca. 30 Ca<sub>xs</sub>:P mole:mole) are higher than K2 (ca. 10). These high ratios make it unlikely that much of the Ca is associated with sinking apatite. This suggests that some Ca is associated with either non-mineral forms or Ca-rich detrital material not accounted for using Al in the sinking material. As such, this could represent an underappreciated mechanism by which Ca is transferred via the biological pump but which does not track calcite or aragonite.

#### 4.2.4. Phytoplankton pigment fluxes and ratios

Of the components that showed decreasing fluxes with depth, many of the phytoplankton pigments were the most rapidly lost

(largest *b* values). Fig. 10 shows selected organic carbon-normalized pigment fluxes at both sites, and Table 3 contains the absolute flux values for all pigments. As noted above and in Buesseler et al., 2007a, Chl *a* showed a distinctly faster attenuation with depth than any other component of sinking material. Also, the flux of Chl *a* appeared to be attenuated less at K2, along with all other components, than at ALOHA. The rest of the pigments shown in Fig. 10 illustrate, however, that not all pigments are equally degraded during transport through the mesopelagic and that there are site-to-site differences as well. For example, 19'-butanoyloxyfucoxanthin (But), was observed to attenuate faster than Chl *a* at ALOHA (so much so that no But was found in the 500 m traps), while it appears to attenuate at about the same rate as Chl *a* at K2. Similar behavior was shown by 19'-hexanoyloxyfucoxanthin (Hex) and chlorophyll *c* (Chl *c*). No accessory pigments were seen to significantly increase in flux relative to POC at ALOHA, with alpha carotene ( $\alpha$  Car), beta carotene ( $\beta$  Car, not shown), fucoxanthin (Fuco) and zeaxanthin (Zeax) possibly showing increases relative to POC at K2. Another notable site difference was that peridinin (Per, a dinoflagellate pigment) was not found in the sediment traps at K2.

The absolute pigment fluxes, and the water column ecosystems that are the source of sinking particles, are markedly different at the two sites. Station ALOHA exhibited higher fluxes and concentrations of Per, violaxanthin (Viola), Zeax, monovinyl chlorophyll *b* (MV-Chl *b*), a Car and divinyl chlorophyll *a* (DV-Chl *a*), and higher relative pigment fluxes for all except Fuco and Chl *c*, with Hex and diadinoxanthin (DDX) being roughly comparable at both sites. Indeed, Per and Viola were not observed in the trap material at K2, even though Per was found in the water column. Fuco and Chl *c* are pigments associated with diatoms, and it is not surprising therefore that the diatom-dominated producer community at K2 would therefore produce more absolute and relative amounts of these pigments. Similarly, the higher abundances of Per and Zeax highlight the greater role of small cells such as dinoflagellates and cyanobacteria at ALOHA. The greater relative abundance of pigments at ALOHA may also confirm the greater overall diversity of producers at ALOHA than at K2.

Though the phytoplankton pigments appeared to attenuate in flux faster than most other components, they did tend to show less attenuation at K2 than at ALOHA, in a similar manner to the other biogenic components. Fucoxanthin is a particularly good example of this. That pigment exhibited the largest *b* value of any component at ALOHA as well as the largest change in *b* between the two sites. This indicates that fucoxanthin went from being one of the most attenuated pigments to one of the least. As this pigment is always associated with diatoms and therefore the same sort of primary material from which the sinking fluxes were drawn, this dramatic shift in attenuation highlights the differences in ecosystem and mesopelagic processing between these two sites.

#### 4.2.5. Flux characteristics 2: increasing fluxes with depth

Though the Al (and other crustal components) were consistent with dust input at 150 m (see below Section 4.2.7), their fluxes increased with depth at K2 but not at ALOHA. As explored in greater detail in other papers, this flux increase, along with suspended particle data suggest that a lateral plume from the continental shelf is responsible for an additional supply of Al and other elements below 150 m (ca. 50%; Lam and Bishop, 2008; Lamborg et al., this volume; J. Bishop, pers. comm.). For example, substantial maxima in suspended Fe and Mn concentrations were observed from 100 to 200 m, a depth/density corresponding to nearby shelf/slopes, and with trap collected material having crustal Fe/Al ratios but enhanced Mn/Al ratios. These observations

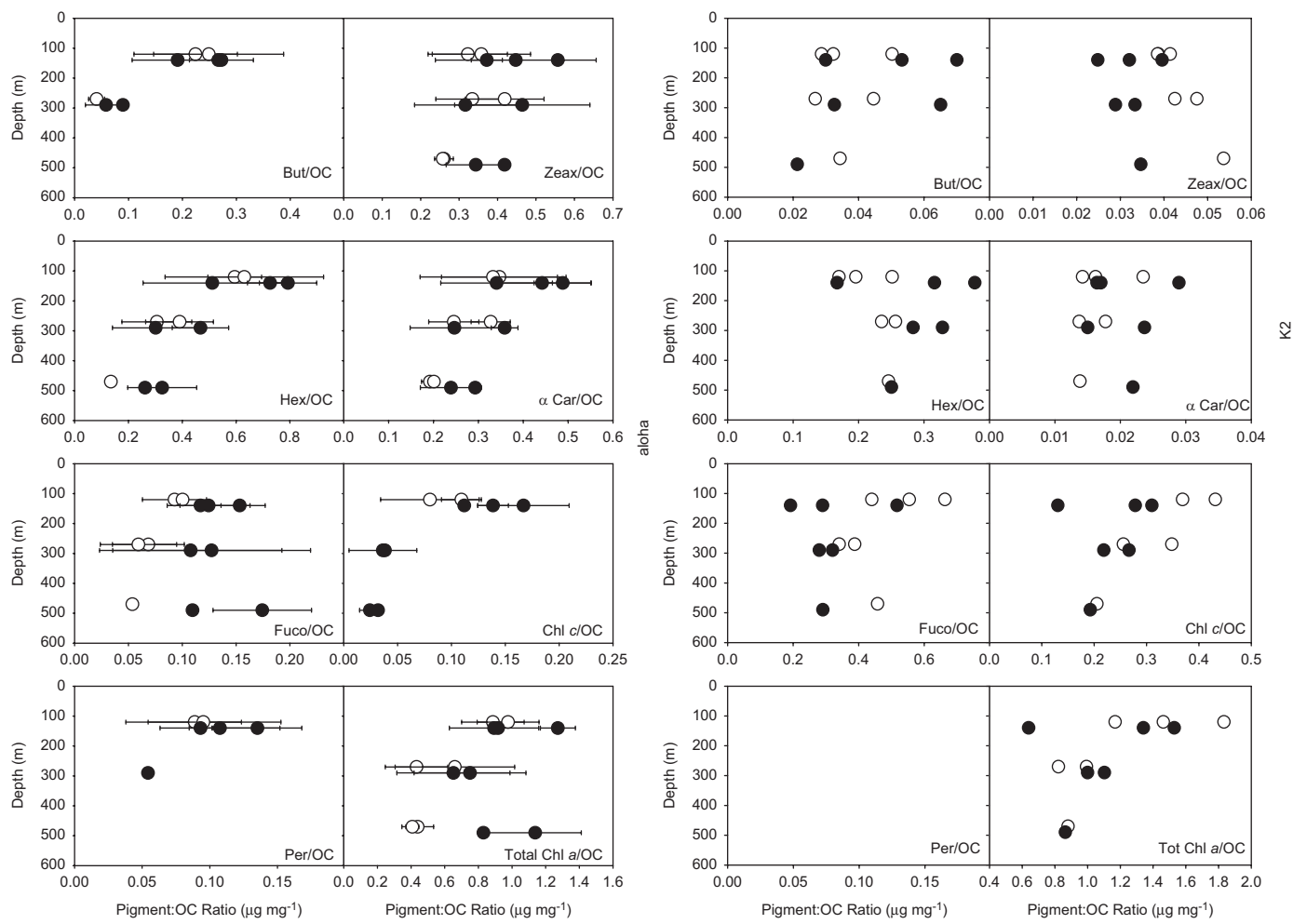


**Fig. 10.** Summary of the fluxes of phytoplankton pigments at ALOHA (left) and K2 (first deployment depicted shallower and in white), normalized to organic carbon.

are consistent with mobilization of material from continental margins having undergone some post-depositional diagenetic alteration (e.g., Marin and Giresse, 2001; Johnson et al., 2003).

The other element observed to have increasing fluxes, but at both sites, was Ba. This is presumed to be the result of *in situ* generation of particulate Ba as a result of organic sulfur oxidation and/or celestite dissolution in sinking particles leading to supersaturation and precipitation of  $\text{BaSO}_4$  (barite; e.g., Dehairs et al., 1980; Bishop, 1988; Bernstein et al., 1998; Dehairs et al., this volume). Sr substitution in barite appears to lower barite solubility (e.g., Monnin and Cividini, 2006) and therefore in degrading marine particles that bear solubilizing celestite (as our do), the presence of relatively high levels of Sr might therefore enhance the formation of particulate Ba. However, no correlation was seen between Sr and Ba at either site that would support this mechanism.

There were correlations between Ba and Al at both sites ( $r^2 = 0.60$  and 0.83 at ALOHA and K2, respectively; Fig. 11), with slopes well above Ba crustal abundance ( $7.4 \times$  and  $27 \times$  at ALOHA and K2; Wedepohl, 1995). The greater degree of Ba:Al enrichment at K2 relative to ALOHA is consistent with the larger export and remineralization of organic carbon at that site (e.g., Dehairs et al., 1991; Dymond and Collier, 1996; Jeandel et al., 2000; Dehairs et al., this volume). However, Ba/Al ratios at 300 and 500 m at K2 show the same slope and high correlation, while the 150 m samples show little correlation. Since much of the Al arriving in the deeper traps at K2 is the result of lateral inputs, it is possible that some of the Ba in these samples is arriving via lateral

transport as well. This would explain the correlation with Al, and the enrichment would presumably be the result of enrichment in biogenic particulate Ba that occurred in the shelf region that supplied the enhanced particulate Al. If this is the case, then it would appear that relatively little additional biogenic barite found its way into the deeper K2 sediment traps. Alternate explanations include Ba uptake onto organic coating associations on aerosols (Murray and Leinen, 1993) and/or onto Fe-oxides of dust particles (Schroeder et al., 1997) or enhanced scavenging of dissolved Al onto the sinking particles (e.g., Murray et al., 1993; Kryc et al., 2003). Unfortunately, we do not currently have particulate Al data to compare with the scavenging rates of Mn to confirm the lateral plume as the source of Al in the deeper traps. In another report in this volume, Dehairs and colleagues explore the cycling of particulate Ba during VERTIGO in detail.

The flux of lithogenic-associated material did not change in concert with the biogenic phases. For example, at ALOHA, the flux of Al did not change vertically, and at K2, the fluxes did not change between deployments. This suggests that either lithogenic material flux profiles reflect the balance between scavenging-disaggregation-rescavenging by the major sinking phases, or little effective scavenging of this material by the major phases at all. Dust particles, as well as those associated with the lateral plume at K2 are small (a few microns) and would therefore have very slow effective sinking rates on their own (e.g., Lam et al., 2006). Dividing the measured sediment trap fluxes for Al by the estimated slow sinking rates for such small particles suggests steady-state particulate pools very similar to those measured by

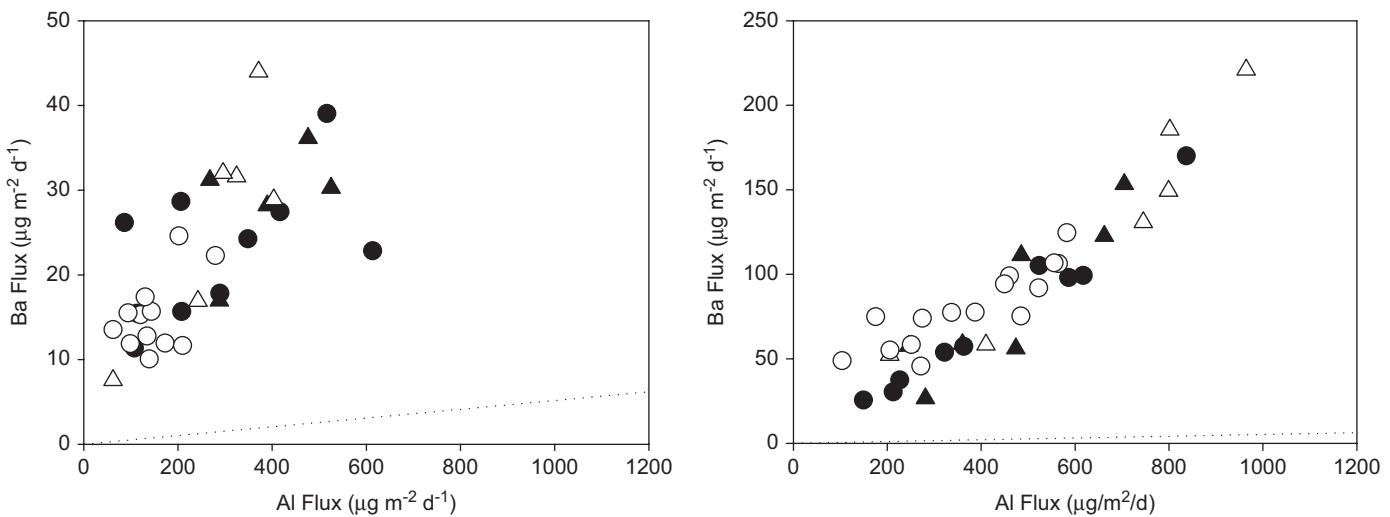


**Fig. 11.** Correlations of total Ba with Al in the NBST (circles) and Clap Traps (triangles) at ALOHA (left) and K2. First deployment in black, second in white. The dotted lines represent the Ba:Al crustal ratio reported by Wedepohl (1995).

*in situ* pumps (Bishop, pers. comm.). Taken together, this information suggests that such small particles are not scavenged very effectively. While sinking aggregates may act as “nets” for other particle types (Passow and De La Rocha, 2006), it appears that lithogenics may slip through these nets.

#### 4.2.6. Flux ratios

The OC:N and OC:P relationships for both sites are shown in Fig. 12. The nutrient–nutrient figures contain data from samples at all depths, deployments and sampling devices, and describe the remineralization ratios of macronutrients during flux attenuation at our sampling sites. The general trend of lower fluxes at deeper depths is represented in these figures, but the nutrient correlations are observed to hold at all depths regardless of the absolute nutrient flux. This is readily seen in the case of K2 where the 2nd deployment fluxes were much lower than the first, and some 150 m nutrient fluxes in the 2nd deployment were lower than 500 m fluxes in the first. It is also interesting to note that the OC:N ratios at both sites (8.5) and OC:P ratios at ALOHA ( $221 \pm 23$ ) are substantially above typical Redfield values. This is not surprising as the detritus that makes up sinking marine particles (e.g., fecal pellets, exopolymers, plankton hard parts) tend to be N and P poor (e.g., Knauer et al., 1979). The OC:P relationship at K2, however, shows slopes that are either equivalent to Redfield (deployment 1;  $114 \pm 23$ ), or substantially below the canonical value of 106 (deployment 2;  $62 \pm 8$ ). Both deployments at K2 also showed significant intercept values to the C/N relationship ( $1.3 \pm 0.5$  mmole OC;  $0.6 \pm 0.1$  mmole OC). It is also worth noting the higher degree of correlation between OC and N than OC with P. As much of the P pool within living cells is in the form of highly soluble adenosine phosphates and N is intimately associated to OC in a variety of molecules, leakage of P during feeding and diffusion from aggregated material could explain the greater variability in OC:P than OC:N.

It is difficult to fit the data with a model based on intrinsically different remineralization length scales for OC and N, which has been the typical approach to explain changing OC:N ratios with depth (e.g., Schneider et al., 2003). This is because allowing OC and N fluxes to be parameterized separately as a function of depth (power-law curves with different  $b$  values for OC and N) predicts a changing slope in a OC:N plot with depth, and this is not seen (Fig. 13). It must be said that the very lowest fluxes at ALOHA hint at a changing slope, but the majority of flux attenuation has occurred by that point, as indicated by the similarity of the OC and

N fluxes in deep traps (David Karl, pers. comm.). If OC and N were cycling independently, they would appear to have nearly identical remineralization length scales. It appears to us, therefore, that alternative models must be used to explain the OC:N data. One alternative is that of a multi-component sinking particle pool; namely that the flux is composed of different kinds of particles, some more degradable than others, each with their own intrinsic organic matter loads and OC/N ratios. Such a model would explain, for example, the linear nature of the nutrient remineralization curves as well as the intercept value at ALOHA. In that situation, the slope would describe the OC/N ratio of the most degradable component, while the intercept value would indicate the existence of a small amount of organic carbon flux associated with high OC/N material that is fairly refractory. This linear OC/N behavior would also be observed if the various components also had inherently different sinking rates, as apparent “degradability” resulting in the attenuation of vertical flux is the balance between the rate of degradation and the rate of sinking. Such a multi-component model has been invoked before to explain OC:bio-mineral correlations in bathypelagic sediment trap data sets (e.g., Armstrong et al., 2002; François et al., 2002; Klaas and Archer, 2002) as well as flux throughout the water column (Lutz et al., 2002).

Visual and chemical observation of the sediment trap material suggests a number of ways in which the various “components” could be assigned. For example, and as alluded to earlier, the various chemical phases that comprise the majority of sample mass (organic material, calcium carbonate, biogenic silica and lithogenic particles) could and have been used to parameterize OC flux. We suggest that it is equally valid to posit particle type (e.g., fecal pellet, aggregate) as the fundamental property that controls the extent to which chemicals are transferred through the twilight zone. This could be done in the context of a model by assigning either inherent degradabilities or sinking rates to the various particle types, as well as chemical compositions. Such a view is similar to that of the foodweb/export model of Michaels and Silver (1988), wherein large grazers are implicated in generating large pellets that enhance export flux. This is not to say that small producer cells are excluded from contributing to material flux because they may not sink quickly. Indeed, recent modeling suggests that picoplankton contribute material to sinking fluxes from the euphotic zone in proportion to their contribution to primary production (Richardson and Jackson, 2007). However, the picoplankton contribution could be

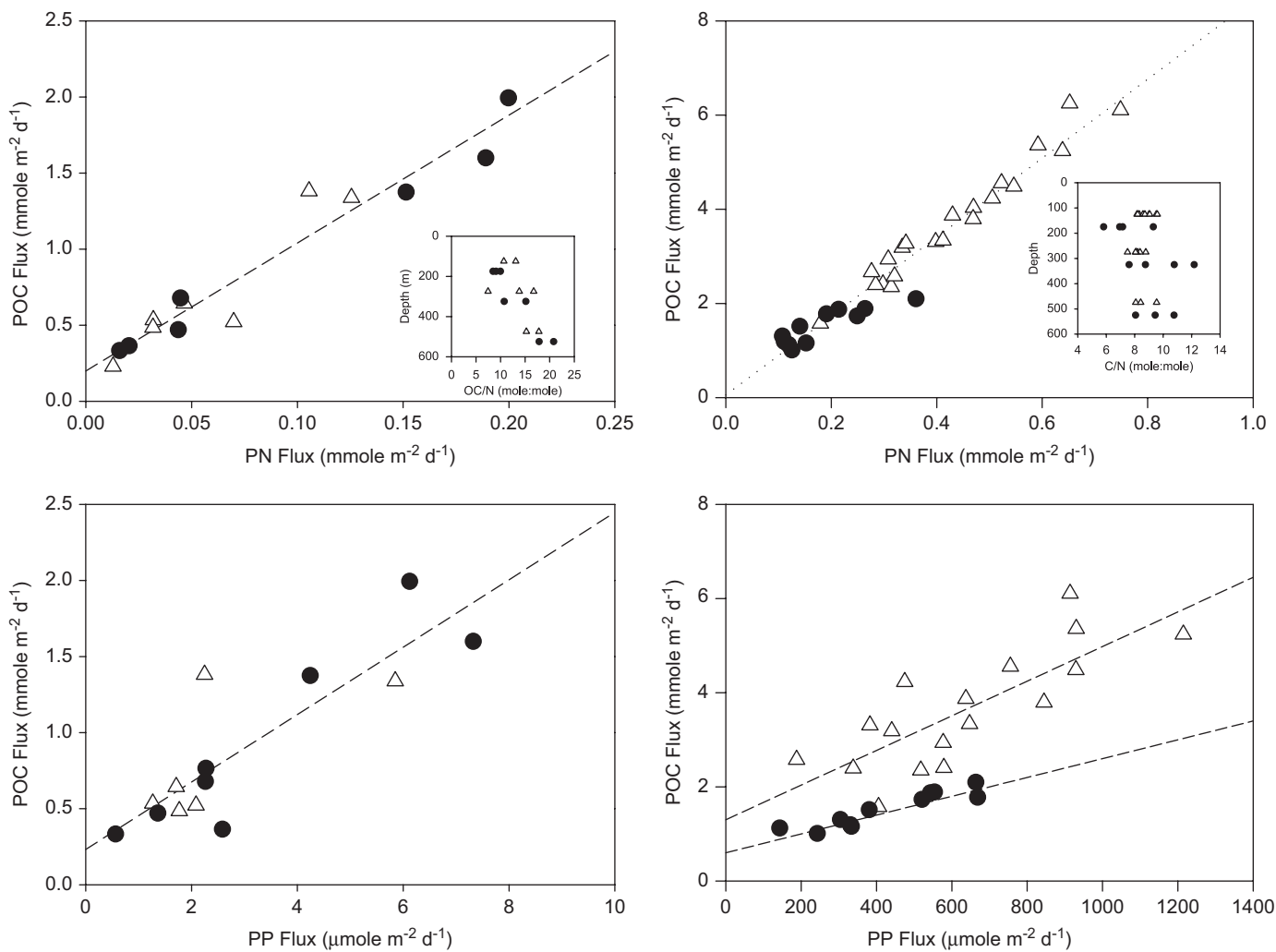


**Fig. 12.** Correlations between organic carbon, total nitrogen and total phosphorus fluxes in NBSTs from ALOHA (left) and K2. First deployment samples are shown in triangles. The results from the formalin and Hg poisoned trap tubes are shown separately here (when available) to increase the sample size and illustrate the tight correlation of OC and N in the samples. Fewer samples are available for comparison at ALOHA due to fewer PIC analyses. Neither site possessed a statistically significant intercept, though ALOHA had a numerically larger value than did K2.

associated with quickly sinking fecal pellets or aggregates, as observed during VERTIGO (M. Silver, pers. comm.), which would still allow grazer community composition to be influential on overall fluxes. Thus, our observations of flux attenuation suggest that the characteristics of sinking material, as set by foodweb structure, have a strong influence on particle dynamics that extends below the euphotic zone, and may play a prominent role in determining mesopelagic transfer efficiency and therefore the overall efficiency of the biological pump.

The POC/PIC ratios are comparable to, or much higher at K2 than at ALOHA (Fig. 14). This is important as the formation of CaCO<sub>3</sub> hard parts releases CO<sub>2</sub>, partially offsetting primary production as a sink for CO<sub>2</sub> (e.g., Holligan and Robertson, 1996). On average, 10% of ALOHA POC flux at 500 m was offset by PIC-related CO<sub>2</sub> emissions, while only 4% at K2 (using a PIC to CO<sub>2</sub> stoichiometry of 0.6; e.g. Frankignoulle et al., 1994). Though there was an attenuation of PIC flux with depth at both sites, it tended to be the least diminished of the biominerals during its transit of the mesopelagic. In general agreement with a recent revised carbonate budget (Berelson et al., 2007), we observed only about half or less of the carbonate entering the mesopelagic was lost to solution. However, the POC/PIC ratios in the mesopelagic zone observed during VERTIGO are much larger than those presented by Berelson and colleagues in their sensitivity analyses, which

suggests a smoother transition between the mesopelagic and bathypelagic zones. This would therefore imply a much lower effective alkalinity flux, from the dissolution of carbonates in the mesopelagic, than their budget suggests, presumably implicating greater supply of alkalinity from dissolution in relatively shallow sediments.

#### 4.2.7. Flux characteristics 3: constant flux with depth (dust-derived material)

As noted in Section 4.2.2, the measured Al flux (~0.3 mg Al m<sup>-2</sup> d<sup>-1</sup> at ALOHA; and for 150 m at K2) can be used to estimate a flux of dust-derived lithogenic material, assuming it is the primary source of Al (4 mg dust m<sup>-2</sup> d<sup>-1</sup>; 7.96% Al/mass; Wedepohl, 1995). This value is consistent with an estimate of dust input to the region based on aerosol measurements and estimates of dry deposition velocity (1.2–12 mg dust m<sup>-2</sup> d<sup>-1</sup>; e.g., Duce et al., 1991; Zieman et al., 1995) and dissolved Al concentrations in regional surface waters (0.3–1.6 mg dust m<sup>-2</sup> d<sup>-1</sup>; Measures and Vink, 2000; Measures et al., 2005). Furthermore, trace elements whose inputs to the ocean are thought to be dominated by dust showed good correlations with Al at ALOHA and in proportions similar to those of crustal materials (Lamborg et al., this volume). The flux of Al and the other apparently dust-derived components at ALOHA were essentially constant with depth, suggesting the

supply and removal of dust-derived lithogenic material was in steady state during our sampling. As with ALOHA, the 150 m Al fluxes at K2 were consistent with atmospheric dust input as a primary source ( $<0.6 \text{ g m}^{-2} \text{ yr}^{-1}$ ; Measures et al., 2005). Though Asian dust plumes sometimes move over the region, flux measurements at ALOHA and K2 and estimates at ALOHA based on dissolved Al, both suggest there was not a large amount of dust deposition to the region during, or immediately preceding our respective occupations of these sites.

## 5. Conclusions

By using multiple new free vehicle sampling platforms (NBSTs), we have collected sinking particulate material from two

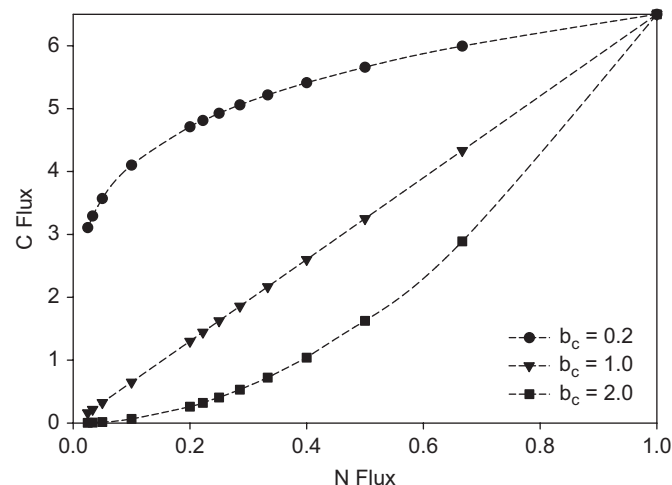


**Fig. 13.** A model of organic carbon and nitrogen fluxes in the mesopelagic based on power-law functional forms and separate  $b$  values. The ratio of organic carbon to nitrogen flux would be represented by  $F_C/F_N = F_{C100}/F_{N100}(z/100)^{b_N-b_C}$ . The figure shows 3 cases where the value of  $b_N$  is set to 1, and the value of  $b_C$  is varied. The flux ratio at 100 m is set to 1. If the values of  $b$  for C and N are very different, the C/N plot becomes noticeably non-linear. Given that field data are rarely this precise, the non-linear curves could appear as straight lines, but differ from the  $b_N = b_C$  case by not appearing to pass through the origin. The C/N plots from VERTIGO look very straight and have very small y intercepts, describing situations that are indistinguishable from that where C and N have the same  $b$  values.

very different oceanic systems and presented well-resolved flux profiles for a number of components. Our solubilization experiments conducted by holding poisoned trap material at ambient temperatures indicated that the relatively short deployment times and rapid processing protocols employed during VERTIGO resulted in relatively little loss of particulate material to the solution phase. Wet splitting at sea, a central part of our processing protocols, was also highly effective at generating equivalent subsamples, facilitating the eventual comparison of the variety of determinations made on the splits. The NBSTs and tethered Clap Traps were still plagued by the incidental collection of zooplankton "swimmers," but we found wet screening of samples prior to splitting to be fairly effective at removing this potential artifact. We note that not all locations may be amenable to this approach if small swimmers pass through the screen, so microscopic examination is still needed, but screening is certainly simpler than picking and easier to conduct in a trace metal clean fashion. We found little difference between the elemental analyses performed on samples poisoned/preserved with either formalin or Hg, though formalin performed better for the preservation of samples for microscopic/biological examination. The two trapping devices employed during VERTIGO agreed with one another fairly well. Qualitatively, the composition of particles collected by the two systems was very comparable, indicating little particle sorting took place. Quantitatively, the two types of devices agreed in 3 of the 4 deployments, disagreeing during the 1st deployment at K2. We noted that this was the deployment during which the highest flux of biogenic material was observed, and during which we suspect that the Clap Traps undersampled by approximately 50% at 150 and 300 m.

At both sites, profiles included examples of decreasing, increasing and constant fluxes as a function of depth. The biogenic components of flux generated in the euphotic zone, including particulate organic matter, phytoplankton pigments, biogenic silica and calcium carbonate all decreased with depth. Increasing fluxes vs. depth were observed for particulate Ba, as a result of the formation of barite, presumably during particle degradation, and for Al and other crustal components at K2 due to scavenging of particles from a plume of material with a continental shelf/slope origin. Constant fluxes vs. depth were observed at ALOHA for Al and other elements, indicating a lithogenic fraction nearly in steady state with dust deposition.

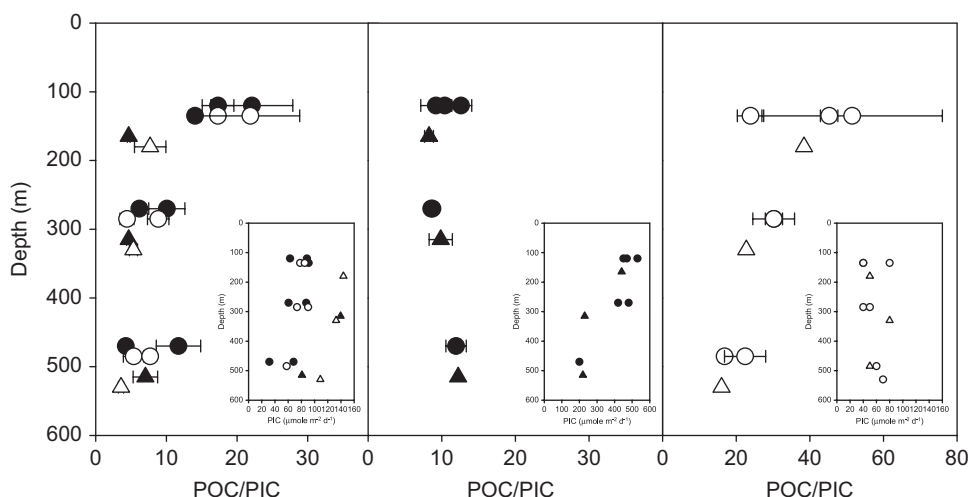


**Fig. 14.** The particulate organic carbon (POC) to particulate inorganic carbon (PIC) "rain ratio" at both sites. NBSTs are depicted by circles, and the first deployments are shown with black circles. The data are shown at different depths for clarity, but all traps were deployed to the same nominal depths. ALOHA (left) and K2 1st deployment (center) exhibit similar rain ratios, while the 2nd deployment at K2 (right) had a much higher ratio throughout the mesopelagic.

The flux of lithogenic-associated material did not change in concert with the biogenic phases. For example, at ALOHA, the sinking flux of Al did not change vertically even though POC and other phases dropped off substantially, and at K2, Al fluxes did not change between deployments even when POC fluxes did. Dust particles, as well as those associated with the lateral plume at K2 are small (a few microns) and would therefore have very slow effective sinking rates on their own (e.g., Lam et al., 2006). While sinking aggregates may act as “nets” for other particle types (Passow and De La Rocha, 2006), it appears that lithogenics may slip through these nets. It has also been suggested that pellets (and therefore active scavenging by grazing zooplankton) are the principal vector for the removal of lithogenic particles (e.g., Deuser et al., 1983). If grazing is the principal removal mechanism for this material, then the behavior at K2 could be consistent if zooplankton were removing dust particles as fast as they enter the ocean. Thus, changing production and POC flux would have no effect on lithogenic flux. At ALOHA, however, this explanation seems inadequate, as the substantial degradation of the sinking organic matter does not seem to be accompanied by a decrease in the Al flux, or an increase in suspended lithogenic material that would be expected to be released by degrading biogenic particles. Thus, at ALOHA, lithogenics and biogenics may be nearly decoupled. This behavior may have only been effective during our occupation, as others have noted seasonal changes in lithogenic scavenging associated with physical and biological trends (e.g., Migon et al., 2002).

The two sites sampled differ greatly in their flux attenuation profiles for the major phases of organic matter, opal, calcium carbonate and lithogenics, with the colder and diatom-dominated K2 site exhibiting much less attenuation for all phases. We contend that this could result of inherently less degradable sinking material, faster sinking rates associated with larger particles (mostly large fecal pellets) and with those being the result of large phytoplankton grazed by large zooplankton. This implies that the ecosystem/flux conceptual model of Michaels and Silver might well extend below the euphotic zone and provide insight into the flux attenuation properties of the twilight zone.

## Acknowledgments

Thanks to Jim Bishop, Phil Boyd, Frank Dehairs, Bill Fitzgerald, Meagan Eagle Gonreea, Paul Henderson, Makio Honda, David Karl, Phoebe Lam, Rob Mason, Devin Ruddick, captains and crews of the R/V *Kilo Moana* and *Roger Revelle*. Special thanks to Rod Johnson for supplying Sargasso seawater used for trap brines, and Rich Zuck for building the splitter.

## References

- Andreev, A.G., Kusakabe, M., 2001. Interdecadal variability in dissolved oxygen in the intermediate water layer of the Western Subarctic Gyre and Kuril Basin (Okhotsk Sea). *Geophysical Research Letters* 28 (12), 2453–2456.
- Antia, A.N., 2005. Particle-associated dissolved elemental fluxes: revising the stoichiometry of mixed layer export. *Biogeosciences Discussions* 2, 275–302.
- Antia, A.N., Koeve, W., Fischer, G., Blanz, T., Schulz-Bull, D., Scholten, J., Neuer, S., Kremling, K., Kuss, J., Peinert, R., Hebbeln, D., Bathmann, U., Conte, M., Fehner, U., Zeitzschel, B., 2001. Basin-wide particulate carbon flux in the Atlantic Ocean: regional export patterns and potential for atmospheric CO<sub>2</sub> sequestration. *Global Biogeochemical Cycles* 15 (4), 845–862.
- Armstrong, R.A., Lee, C., Hedges, J.I., Honjo, S., Wakeham, S.G., 2002. A new, mechanistic model for organic carbon fluxes in the ocean based on the quantitative association of POC with ballast minerals. *Deep-Sea Research Part II-Topical Studies in Oceanography* 49 (1–3), 219–236.
- Berelson, W.M., Balch, W.M., Najjar, R., Feely, R.A., Sabine, C., Lee, K., 2007. Relating estimates of CaCO<sub>3</sub> production, export, and dissolution in the water column to measurements of CaCO<sub>3</sub> rain into sediment traps and dissolution on the sea floor: a revised global carbonate budget. *Global Biogeochemical Cycles* 21 (1), Art. No. GB1024.
- Bernstein, R.E., Byrne, R.H., Schijf, J., 1998. Acantharians: a missing link the oceanic biogeochemistry of barium. *Deep-Sea Research I* 45, 491–505.
- Bidigare, R.R., Kennicutt II, M.C., Brooks, J.M., 1985. Rapid determination of chlorophyll and their degradation products by high-performance liquid chromatography. *Limnology and Oceanography* 30 (2), 432–435.
- Bidle, K.D., Azam, F., 1999. Accelerated dissolution of diatom silica by marine bacterial assemblages. *Nature* 397, 508–512.
- Bingham, F.M., Lukas, R., 1996. Seasonal cycles of temperature, salinity and dissolved oxygen observed in the Hawaii Ocean time-series. *Deep Sea Research II* 43 (2–3), 199–213.
- Bishop, J.K.B., 1988. The Barite-Opal-Organic Carbon Association in oceanic particulate matter. *Nature* 332 (6162), 341–343.
- Boyd, P.W., Gall, M.P., Silver, M.W., Bishop, J.K.B., this volume. Quantifying the surface-subsurface biogeochemical coupling during the VERTIGO ALOHA and K2 studies. *Deep-Sea Research II* [doi:10.1016/j.dsr2.2008.04.010].
- Buesseler, K.O., 1991. Do upper-ocean sediment traps provide an accurate record of particle-flux. *Nature* 353 (6343), 420–423.
- Buesseler, K.O., 1998. The decoupling of production and particulate export in the surface ocean. *Global Biogeochemical Cycles* 12 (2), 297–310.
- Buesseler, K.O., Michaels, A.F., Siegel, D.A., Knap, A.H., 1994. A 3-dimensional time-dependent approach to calibrating sediment trap fluxes. *Global Biogeochemical Cycles* 8 (2), 179–193.
- Buesseler, K.O., Steinberg, D.K., Michaels, A.F., Johnson, R.J., Andrews, J.E., Valdes, J.R., Price, J.F., 2000. A comparison of the quantity and composition of material caught in a neutrally buoyant versus surface-tethered sediment trap. *Deep-Sea Research Part I-Oceanographic Research Papers* 47 (2), 277–294.
- Buesseler, K.O., Andrews, J.E., Pike, S.M., Charette, M.A., Goldson, L.E., Brzezinski, M.A., Lance, V.P., 2005. Particle export during the southern ocean iron experiment (SOFeX). *Limnology and Oceanography* 50 (1), 311–327.
- Buesseler, K.O., Antia, A.N., Chen, M., Fowler, S.W., Gardner, W.D., Gustafsson, O., Harada, H., Michaels, A.F., Rutgers van der Loeff, M., Sarin, M., Steinberg, D.K., Trull, T., 2007a. An assessment of the use of sediment traps for estimating upper ocean particle fluxes. *Journal of Marine Research* 65, 345–416.
- Buesseler, K.O., Lamborg, C.H., Boyd, P.W., Lam, P.J., Trull, T.W., Bidigare, R.R., Bishop, J.K.B., Casciotti, K.L., Dehairs, F., Elskens, M., Honda, M.C., Karl, D.M., Siegel, D., Silver, M.W., Steinberg, D.K., Valdes, J.R., Van Mooy, B., Wilson, S., 2007b. Revisiting carbon flux through the ocean's twilight zone. *Science* 316, 567–570.
- Buesseler, K.O., Trull, T.W., Steinberg, D.K., Silver, M.W., Siegel, D.A., Saitoh, S.-I., Lamborg, C.H., Lam, P.J., Karl, D.M., Jiao, N.Z., Honda, M.C., Elskens, M., Dehairs, F., Brown, S.L., Boyd, P.W., Bishop, J.K.B., Bidigare, R.R., this volume. VERTIGO (VERTical Transport In the Global Ocean): a study of particle sources and flux attenuation in the North Pacific. *Deep-Sea Research II* [doi:10.1016/j.dsr2.2008.04.024].
- Butman, C.A., 1986. Sediment trap biases in turbulent flows: results from a laboratory flume study. *Journal of Marine Research* 44 (645–693).
- Collier, R., 1991. Analysis of particulate matter collected by sediment traps and from sediment cores. In: Hurd, D.C., Spencer, D.W. (Eds.), *Geophysical Monograph 63. Marine Particles: Analysis and Characterization*. American Geophysical Union, Washington, DC.
- Dehairs, F., Chesselet, R., Jedwab, J., 1980. Discrete suspended particles of barite and the barium cycle in the open ocean. *Earth and Planetary Science Letters* 49 (2), 528–550.
- Dehairs, F., Stroobants, N., Goeyens, L., 1991. Suspended barite as a tracer of biological-activity in the Southern-Ocean. *Marine Chemistry* 35 (1–4), 399–410.
- Dehairs, F., Jacquet, S., Savoye, N., Bishop, J., Van Mooy, B., Buesseler, K., Lamborg, C., Elskens, M., Boyd, P., Casciotti, K., Baeyens, W., this volume. Barium in Twilight Zone suspended matter as a potential proxy for particulate organic carbon remineralization: results for the North Pacific. *Deep-Sea Research II* [doi:10.1016/j.dsr2.2008.04.020].
- Deuser, W.G., Brewer, P.G., Jickells, T.D., Commeau, R.F., 1983. Biological control of the removal of abiogenic particles from the surface ocean. *Science* 21, 388–391.
- Duce, R.A., Liss, P.S., Merrill, J.T., Atlas, E.L., Buat-Menard, P., Hicks, B.B., Miller, J.M., Prospero, J.M., Arimoto, R., Church, T.M., Ellis, W., Galloway, J.N., Hansen, L., Jickells, T.D., Knap, A.H., Reinhardt, K.H., Schneider, B., Soudine, A., Tokos, J.J., Tsunogai, S., Wollast, R., Zhou, M., 1991. The atmospheric input of trace species to the world ocean. *Global Biogeochemical Cycles* 5, 193–259.
- Ducklow, H.W., Steinberg, D.K., Buesseler, K.O., 2001. Upper ocean carbon export and the biological pump. *Oceanography* 14 (4), 50–58.
- Dymond, J., Collier, R., 1996. Particulate barium fluxes and their relationships to biological productivity. *Deep-Sea Research Part II-Topical Studies in Oceanography* 43 (4–6), 1283.
- Elskens, M., Brion, N., Buesseler, K., Van Mooy, B.A.S., Boyd, P., Dehairs, F., Savoye, N., Baeyens, W., this volume. Primary, new and export production in the N.W. Pacific Subarctic gyre during the VERTIGO K2 experiments. *Deep-Sea Research II* [doi:10.1016/j.dsr2.2008.04.013].
- Feely, R.A., Sabine, C.L., Lee, K., Millero, F.J., Lamb, M.F., Greeley, D., Bullister, J.L., Key, R.M., Peng, T.H., Kozyr, A., Ono, T., Wong, C.S., 2002. In situ calcium carbonate dissolution in the Pacific Ocean. *Global Biogeochemical Cycles* 16 (4), 1144.
- Finkel, Z.V., Quigg, A., Raven, J.A., Reinfelder, J.R., Schofield, O.E., Falkowski, P.G., 2006. Irradiance and the elemental stoichiometry of marine phytoplankton. *Limnology and Oceanography* 51 (6), 2690–2701.

- François, R., Honjo, S., Krishfield, R., Manganini, S., 2002. Factors controlling the flux of organic carbon to the bathypelagic zone of the ocean. *Global Biogeochemical Cycles* 16 (4), 1087–1106.
- Frankignoulle, M., Canon, C., Gattuso, J.P., 1994. Marine calcification as a source of carbon dioxide: positive feedback of increasing atmospheric CO<sub>2</sub>. *Limnology and Oceanography* 39 (2), 458–462.
- Gardner, W.D., 2000. Sediment trap sampling in surface waters. In: Hanson, R.B., Ducklow, H.W., Field, J.P. (Eds.), *The Changing Ocean Carbon Cycle: A Midterm Synthesis of the Joint Global Ocean Flux Study*. Cambridge University Press, New York, pp. 240–281.
- Gust, G., Michaels, A.F., Johnson, R., Deuser, W.G., Bowles, W., 1994. Mooring line motions and sediment trap hydromechanics—in-situ intercomparison of 3 common deployment designs. *Deep-Sea Research Part I-Oceanographic Research Papers* 41 (5–6), 831–857.
- Gust, G., Bowles, W., Giordano, S., Huttel, M., 1996. Particle accumulation in a cylindrical sediment trap under laminar and turbulent steady flow: an experimental approach. *Aquatic Sciences* 58 (4), 297–326.
- Hedges, J.I., Lee, C., Wakeham, S.G., Hernes, P.J., Peterson, M.L., 1993. Effects of poisons and preservatives on the fluxes and elemental compositions of sediment trap materials. *Journal of Marine Research* 51 (3), 651–668.
- Ho, T.Y., Quigg, A., Finkel, Z.V., Milligan, A.J., Wyman, K., Falkowski, P.G., Morel, F.M.M., 2003. The elemental composition of some marine phytoplankton. *Journal of Phycology* 39 (6), 1145–1159.
- Holligan, P.M., Robertson, J.E., 1996. Significance of ocean carbonate budgets for the global carbon cycle. *Glob Change Biology* 2 (2), 85–95.
- Honda, M.C., Kawakama, H., Sasaoka, K., Watanabe, S., Dickery, T., 2006. Quick transport of primary produced organic carbon in the ocean interior. *Geophysical Research Letters* 33 (13), L16603.
- Honjo, S., Manganini, S.J., 1993. Annual biogenic particle fluxes to the interior of the North-Atlantic Ocean—studied at 34-degrees-N 21-degrees-W and 48-degrees-N 21-degrees-W. *Deep-Sea Research Part II-Topical Studies in Oceanography* 40 (1–2), 587–607.
- Honjo, S., Francois, R., Manganini, S., Dymond, J., Collier, R., 2000. Particle fluxes to the interior of the Southern Ocean in the Western Pacific sector along 170 degrees W. *Deep-Sea Research Part II-Topical Studies in Oceanography* 47 (15–16), 3521–3548.
- Huang, S., Sholkovitz, E.R., Conte, M.H., 2007. Application of high-temperature fusion for analysis of major and trace elements in marine sediment trap samples. *L&O: Methods* 5, 13–22.
- Jeandel, C., Tachikawa, K., Bory, A., Dehairs, F., 2000. Biogenic barium in suspended and trapped material as a tracer of export production in the tropical NE Atlantic (EUMELI sites). *Marine Chemistry* 71 (1–2), 125–142.
- Jickells, T.D., Newton, P.P., King, P., Lampitt, R.S., Boute, C., 1996. A comparison of sediment trap records of particle fluxes from 19 to 48 degrees N in the northeast Atlantic and their relation to surface water productivity. *Deep-Sea Research Part I-Oceanographic Research Papers* 43 (7), 971–986.
- Johnson, K.M., King, A.E., Sieburth, J.M., 1985. Coulometric TCO<sub>2</sub> analyses for marine studies; an introduction. *Marine Chemistry* 16 (1), 61–82.
- Johnson, K.S., Elrod, V.A., Fitzwater, S.E., Plant, J.N., Chavez, F.P., Tanner, S.J., Gordon, R.M., Westphal, D.L., Perry, K.D., Wu, J.F., Karl, D.M., 2003. Surface ocean–lower atmosphere interactions in the Northeast Pacific Ocean Gyre: aerosols, iron, and the ecosystem response. *Global Biogeochemical Cycles* 17 (2).
- Kahler, P., Bauerfeind, E., 2001. Organic particles in a shallow sediment trap: substantial loss to the dissolved phase. *Limnology and Oceanography* 46 (3), 719–723.
- Karl, D.M., 1999. A sea of change: biogeochemical variability in the North Pacific Subtropical Gyre. *Ecosystems* 2 (3), 181–214.
- Karl, D.M., Knauer, G.A., 1989. Swimmers: a recapitulation of the problem and a potential solution. *Oceanography* April, 32–35.
- Karl, D.M., Bidigare, R.R., Letelier, R.M., 2001a. Long-term changes in plankton community structure and productivity in the North Pacific Subtropical Gyre: the domain shift hypothesis. *Deep Sea Research II* 48 (8–9), 1449–1470.
- Karl, D.M., Bjorkman, K.M., Dore, J.E., Fujieki, L., Hebel, D.V., Houlihan, T., Letelier, R.M., Tupas, L.M., 2001b. Ecological nitrogen-to-phosphorus stoichiometry at station ALOHA. *Deep Sea Research II* 48 (8–9), 1529–1566.
- Klaas, C., Archer, D.E., 2002. Association of sinking organic matter with various types of mineral ballast in the deep sea: implications for the rain ratio. *Global Biogeochemical Cycles* 16 (4), 1116–1129.
- Knauer, G.A., Martin, J.H., Bruland, K.W., 1979. Fluxes of particulate carbon, nitrogen, and phosphorus in the upper water column of the northeast Pacific. *Deep-Sea Research* 26A, 97–108.
- Knauer, G.A., Karl, D.M., Martin, J.H., Hunter, C.N., 1984. In situ effects of selected preservatives on total carbon, nitrogen and metals collected in sediment traps. *Journal of Marine Research* 42, 445–462.
- Kobari, T., Steinberg, D.K., Ueda, A., Silver, M.W., Tsuda, A., Kitamura, M., this volume. Impacts of ontogenetically migrating copepods on downward carbon flux in the western Subarctic Pacific Ocean. *Deep-Sea Research II* [doi:10.1016/j.dsr2.2008.04.016].
- Kryc, K.A., Murray, R.W., Murray, D.W., 2003. Al-to-oxide and Ti-to-organic linkages in biogenic sediment: relationships to paleo-export production and bulk Al/Ti. *Earth and Planetary Science Letters* 211 (1–2), 125–141.
- Kuss, J., Kremling, K., 1999. Particulate trace element fluxes in the deep northeast Atlantic Ocean. *Deep-Sea Research Part I-Oceanographic Research Papers* 46 (1), 149–169.
- Lam, P.J., Bishop, J.K.B., 2008. The continental margin is a key source of iron to the HNLC North Pacific Ocean. *Geophysical Research Letters* 35, Art. No. L07608.
- Lam, P.J., Bishop, J.K.B., Henning, C.C., Marcus, M.A., Waychunas, G.A., Fung, I.Y., 2006. Wintertime phytoplankton bloom in the Subarctic Pacific supported by continental margin iron. *Global Biogeochemical Cycles* 20 (1).
- Lamborg, C.H., Buesseler, K.O., Lam, P.J., Valdes, J.R., Bertrand, C.H., Pike, S., Manganini, S., this volume. Sinking fluxes of minor and trace elements in the North Pacific Ocean measured during the VERTIGO program. *Deep-Sea Research II* [doi:10.1016/j.dsr2.2008.04.012].
- Lee, C., Hedges, J.I., Wakeham, S.G., Zhu, N., 1992. Effectiveness of various treatments in retarding microbial activity in sediment trap material and their effects on the collection of swimmers. *Limnology and Oceanography* 37 (1), 117–130.
- Lutz, M., Dunbar, R., Caldeira, K., 2002. Regional variability in the vertical flux of particulate organic carbon in the ocean interior. *Global Biogeochemical Cycles* 16 (3), 1037.
- Marin, B., Giresse, P., 2001. Particulate manganese and iron in recent sediments of the Gulf of Lions continental margin (north-western Mediterranean Sea): deposition and diagenetic process. *Marine Geology* 172 (1–2), 147–165.
- Martin, J.H., Knauer, G.A., Karl, D.M., Broenkow, W.W., 1987. VERTEX: carbon cycling in the NE Pacific. *Deep-Sea Research* 34, 267–285.
- Measures, C.I., Vink, S., 2000. On the use of dissolved aluminum in surface waters to estimate dust deposition to the ocean. *Global Biogeochemical Cycles* 14 (1), 317–327.
- Measures, C.I., Brown, M.T., Vink, S., 2005. Dust deposition to the surface waters of the western and central North Pacific inferred from surface water dissolved aluminum concentrations. *Geochemistry Geophysics Geosystems* 6.
- Michaels, A.F., Silver, M.W., 1988. Primary production, sinking flux and the microbial food web. *Deep-Sea Research* 35, 473–490.
- Michaels, A.F., Caron, D.A., Swanberg, N.R., Howse, F.A., Michaels, C.M., 1995. Planktonic sarcodines (acantharia, radiolaria, foraminifera) in surface waters near Bermuda—abundance, biomass and vertical flux. *Journal of Plankton Research* 17 (1), 131–163.
- Migon, C., Sandroni, V., Marty, J.C., Gasser, B., Miquel, J.C., 2002. Transfer of atmospheric matter through the euphotic layer in the northwestern Mediterranean: seasonal pattern and driving forces. *Deep-Sea Research Part II-Topical Studies in Oceanography* 49 (11), 2125–2141.
- Monnin, C., Cividini, D., 2006. The saturation state of the world's ocean with respect to (Ba,Sr)SO<sub>4</sub> solid solutions. *Geochimica et Cosmochimica Acta* 70 (13), 3290–3298.
- Mortlock, R.A., Froelich, P.N., 1989. A simple method for the rapid-determination of biogenic opal in pelagic marine-sediments. *Deep-Sea Research Part A-Oceanographic Research Papers* 36 (9), 1415–1426.
- Muller, P.J., Schneider, R., 1993. An automated leaching method for the determination of opal in sediments and particulate matter. *Deep-Sea Research Part I-Oceanographic Research Papers* 40 (3), 425–444.
- Murray, R.W., Leinen, M., 1993. Chemical-transport to the sea-floor of the equatorial Pacific-Ocean across a latitudinal transect at 135-degrees-W—tracking sedimentary major, trace, and rare-earth element fluxes at the Equator and the Intertropical Convergence Zone. *Geochimica et Cosmochimica Acta* 57 (17), 4141–4163.
- Murray, R.W., Leinen, M., Isern, A.R., 1993. Biogenic flux of Al to sediment in the central equatorial Pacific-Ocean—evidence for increased productivity during glacial periods. *Paleoceanography* 8 (5), 651–670.
- Noji, T.T., Borsheim, K.Y., Rey, F., Nortvedt, R., 1999. Dissolved organic carbon associated with sinking particles can be crucial for estimates of vertical carbon flux. *Sarsia* 84 (2), 129–135.
- O'Neill, L.P., Benitez-Nelson, C.R., Styles, R.M., Tappa, E., Thunell, R.C., 2005. Diagenetic effects on particulate phosphorus samples collected using formalin-poisoned sediment traps. *Limnology and Oceanography-Methods* 3, 308–317.
- Passow, U., De La Rocha, C.L., 2006. Accumulation of mineral ballast on organic aggregates. *Global Biogeochemical Cycles* 20 (GB1013, doi:10.1029/2005GB002579).
- Peterson, M.L., Wakeham, S.G., Lee, C., Askea, M.A., Miquel, J.C., 2005. Novel techniques for collection of sinking particles in the ocean and determining their settling rates. *L&O: Methods* 3, 520–532.
- Pohl, C., Löffler, A., Hennings, U., 2004. A sediment trap flux study for trace metals under seasonal aspects in the stratified Baltic Sea (Gotland Basin; 57 degrees 19.20'N; 20 degrees 03.00'E). *Marine Chemistry* 84 (3–4), 143–160.
- Primeau, F., 2006. On the variability of the exponent in the power law depth dependence of POC flux estimated from sediment traps. *Deep Sea Research I* 53, 1335–1343.
- Reid, J.L., 1997. On the total geostrophic circulation of the Pacific Ocean: flow patterns, tracers, and transports. *Progress in Oceanography* 39 (4), 263–352.
- Richardson, T.L., Jackson, G.A., 2007. Small phytoplankton and carbon export from the surface ocean. *Science* 315 (5813), 838–840.
- Santschi, P.H., Murray, J.W., Baskaran, M., Benitez-Nelson, C.R., Guo, L.D., Hung, C.-C., Lamborg, C., Moran, S.B., Passow, U., Roy-Barman, M., 2006. Thorium speciation in seawater. *Marine Chemistry* 100 (3–4), 250–268.
- Schneider, B., Schlitzer, R., Fischer, G., Nothig, E.M., 2003. Depth-dependent elemental compositions of particulate organic matter (POM) in the ocean. *Global Biogeochemical Cycles* 17 (2).
- Schroeder, J.O., Murray, R.W., Leinen, M., Pfleiderer, R.C., Janecek, T.R., 1997. Barium in equatorial Pacific carbonate sediment: terrigenous, oxide, and biogenic associations. *Paleoceanography* 12 (1), 125–146.
- Stanley, R.H.R., Buesseler, K.O., Manganini, S.J., Steinberg, D.K., Valdes, J.R., 2004. A comparison of major and minor elemental fluxes collected in neutrally

- buoyant and surface-tethered sediment traps. *Deep-Sea Research Part I-Oceanographic Research Papers* 51, 1387–1395.
- Steinberg, D.K., Cope, J.S., Wilson, S.E., Kobari, T., this volume. A comparison of mesopelagic mesozooplankton community structure in the subtropical and Subarctic North Pacific Ocean. *Deep-Sea Research II* [[doi:10.1016/j.dsr2.2008.04.025](https://doi.org/10.1016/j.dsr2.2008.04.025)].
- Trull, T.W., Bray, S., Buesseler, K.O., Lamborg, C., Manganini, S., Moy, C., Valdes, J., this volume. In-situ measurement of mesopelagic particle sinking rates and the control of carbon transfer to the ocean interior during the Vertical Flux in the Global Ocean (VERTIGO) voyages in the North Pacific. *Deep-Sea Research II* [[doi:10.1016/j.dsr2.2008.04.021](https://doi.org/10.1016/j.dsr2.2008.04.021)].
- Valdes, J.R., Price, J.F., 2000. A neutrally buoyant, upper ocean sediment trap. *Journal of Atmospheric and Oceanic Technology* 17 (1), 62–68.
- van der Loeff, M.R., Sarin, M.M., Baskaran, M., Benitez-Nelson, C., Buesseler, K.O., Charette, M., Dai, M., Gustafsson, O., Masque, P., Morris, P.J., 2006. A review of present techniques and methodological advances in analyzing  $^{234}\text{Th}$  in aquatic systems. *Marine Chemistry* 100 (3–4), 190–212.
- Volk, T., Hoffert, M., 1985. Ocean carbon pumps: analysis of relative strengths and efficiencies in ocean-driven atmospheric  $\text{CO}_2$  changes. In: Sundquist, E., Broecker, W.S. (Eds.), *The Carbon Cycle and Atmospheric  $\text{CO}_2$ : Natural Variations Archean to Present*. American Geophysical Union, Washington, DC, pp. 99–110.
- Wang, W.X., Reinfelder, J.R., Lee, B.G., Fisher, N.S., 1996. Assimilation and regeneration of trace elements by marine copepods. *Limnology and Oceanography* 41 (1), 70–81.
- Wedepohl, K.H., 1995. The composition of the continental crust. *Geochimica et Cosmochimica Acta* 59 (7), 1217–1232.
- Wilson, S.E., Steinberg, D.K., Buesseler, K.O., this volume. Changes in fecal pellet characteristics with depth as indicators of zooplankton repackaging of particles in the mesopelagic zone of the subtropical and subarctic North Pacific Ocean. *Deep-Sea Research II* [[doi:10.1016/j.dsr2.2008.04.019](https://doi.org/10.1016/j.dsr2.2008.04.019)].
- Wright, S.W., Jeffery, S.W., Mantoura, R.F.C., Llewellyn, C.A., Bjornland, T., Repeta, D., Welschmeyer, N., 1991. Improved HPLC method for the analysis of chlorophylls and carotenoids from marine phytoplankton. *Marine Ecology-Progress Series* 77, 183–196.
- Zieman, J.J., Holmes, J.L., Connor, D., Jensen, C.R., Zoller, W.H., Hermann, D.M., Parrington, J.R., Gordon, G.E., 1995. Atmospheric aerosol trace element chemistry at Mauna Loa observatory. 1. 1979–1985. *Journal of Geophysical Research-Atmospheres* 100 (D12), 25979–25994.